*applied sciences*

MDPI

*Review*

# Deformation Behaviour and Failure Prediction of Additively Manufactured Lattices: A Review and Analytical Approach

**Munashe Ignatius Chibinyani [1,*], Thywill Cephas Dzogbewu [1], Maina Maringa [2] and Amos Mwangi Muiruri [1,2]**

[1] Department of Mechanical and Mechatronics Engineering, Central University of Technology, Bloemfontein 9301, South Africa; tdzogbewu@cut.ac.za (T.C.D.); amuiruri@mut.ac.ke (A.M.M.)
[2] Department of Mechanical Engineering, Muranga University of Technology, Muranga 10200, Kenya; maringa@mut.ac.ke
* Correspondence: chibinyanimunashe@gmail.com

**Abstract**

Cellular structures are well-established in biological materials and are often mimicked in many kinds of structural designs applicable to engineering. This results from their lightweight designs and good mechanical properties. Cellular designs in nature have extremely complex configurations. As a result, the deformation behaviour models for bioinspired hollow parts based on these geometries, that are presently available in the literature, are limited in their capacity to provide detailed descriptions of the mechanisms resulting in deformation. Extensions to the existing deformation behaviour mechanisms of cellular parts are proposed in this paper. First, a general outlook on cellular designs is given. This is followed by a review of the commonly recognised two-stage stress–strain curve for cellular parts and its comparison with the new curve suggested in this paper, which incorporates suggestions more fully accounting for the deformation mechanisms of these structures. Further, analytical models that are available in the literature, outlining the behaviour of cellular parts, are highlighted, together with new models developed here for predicting failure of lattice structures based on the Tresca and von Mises criterion. Next follows a discussion of proposed strategies that could be adopted in deformation behaviour models for optimising the design of hollow structures to improve their mechanical properties. Finally, the anticipated challenges for and future insights into the incorporation of the cellular behaviour models suggested here, in cutting-edge structural design for additive manufacturing (AM), are highlighted.

**Keywords:** cellular structures; biological materials; deformation behaviour; failure criteria; analytical modelling; structural optimisation; additive manufacturing

Check for updates

Academic Editor: Gang Wei

Received: 14 November 2025
Revised: 10 January 2026
Accepted: 12 January 2026
Published: 20 January 2026

**Copyright:** © 2026 by the authors. Licensee MDPI, Basel, Switzerland. This article is an open access article distributed under the terms and conditions of the Creative Commons Attribution (CC BY) license.

## 1. Introduction

Natural cellular structures are particularly useful in numerous structural applications in engineering [1–5]. Organic cellular structures, including the bones of birds or plant stems, have the advantages of being lightweight in design, as well as having good load-bearing capacity [4,6–9]. These structures serve as inspiration for engineers and researchers in the aerospace, automotive, biomedical and architecture [2–4,7,8] industries, as they aid in the design of lightweight parts [2–4,7,8]. These lightweight parts are often related to applications such as aircraft fuselages [6,10], low density vehicle frames [11,12], and towering hollow structures [13,14]. Biological structures such as honeycombs and bone

trabeculae effectively distribute loads, thus reducing stress concentrations [7,15]. Using comparable load-distributing strategies in structural components such as bridge trusses, support beams, and composite materials improves strength and durability [4]. Manufacturers can develop structural parts that maximise the usage of material, minimise waste, and reduce impact on the environment by mimicking nature's efficient cellular designs. This is consistent with the principles of sustainable design and contributes to the development of environmentally friendly technologies [4,15]. Cellular materials, such as trabecular bone in vertebrate structures and the foam-like structure of wood, have good energy absorption properties [7,15]. This characteristic is typically used to generate impact-resistant materials and structures such as protective gear [15], automotive crash structures [12], and protective packaging [3,4,15]. The natural design of cellular parts tends to be adaptable and malleable, thus allowing cellular parts to withstand dynamic loads and harsh environmental changes. This adaptability is useful in engineering applications where structures must adapt to changing conditions or withstand deformation without failing [12,15]. Numerous biological cellular configurations, such as the honeycomb structure in beehives or the structures in particular plant tissues, are good regulators of temperature and thermal insulators [7,15]. Manufacturers adopt these thermal properties to generate structures that provide efficient thermal control, such as building insulation or heat exchangers [3,4,7,15]. Biological cellular designs, such as air-filled chambers in aquatic plant stems or gas-filled bladders in marine animals, allow for buoyancy and flotation [4,7,15]. Comparable concepts for building buoyant materials and structures for marine vessels, floating platforms, and life-saving equipment could potentially be adopted. Specific cellular structures, such as coral reefs and sponge skeletons, have complicated geometries that improve fluid flow and filtering capabilities [7]. The use of the biomimicry concept to generate efficient fluid flow systems, filters, and membranes for use in water treatment, HVAC systems, and advanced manufacturing processes is recommended based on the design of the biological structures mentioned in the previous sentence. It is important to note that cellular designs in nature are often studied to generate specific technological alternatives and novel design concepts [4]. Nature's unique different cellular architectures have been used in developing bioinspired structures for a wide range of industries, including aerospace, architecture, and material science [4,15]. These structures are designed for increased strength, lightweightness, and energy absorption, offering unique solutions for a wide range of applications.

Cellular designs observed in biological materials have phenomenal complexities in their configurations as well as being effective in their mechanical behaviour, which often drives engineers and scientists to build bioinspired hollow designs for various engineering applications [2,16–19]. There has been substantial progress in the development of bioinspired cellular parts, such as metamaterials [20–23] and structural components [1–19]. However, present-day models for the mechanical behaviour of cellular architectures often fall short in their capacity to provide detailed descriptions of the prevailing deformation mechanisms [15]. The following statements highlight a few of the reasons why current behavioural models fall short. The complicated geometries and underlying mechanisms that govern the deformation of these bioinspired cellular parts render it difficult to accurately model their behaviour [16,24–30]. Regardless of advances in modelling techniques such as finite element analysis (FEA) and computational fluid dynamics (CFD), these techniques often simplify geometry or presume idealised conditions but fail to capture the complexity of natural structures [16,24,27–30]. However, such simplifications are needed for computational efficiency and/or analytical tractability [24,30]. To accurately model the behaviour of cellular parts, material properties must often be homogenised, or unit cells considered as uniform structures [28]. Although such approaches can capture general de-

formation behaviour, they overlook heterogeneities within unit cells or changes in localised stresses [16,24,26–30].

In addition, natural cellular structures tend to be hierarchically structured, with complicated physical interactions between unit cells and their environment [15,25,27,28,30]. Capturing these intricacies in behaviour models requires advanced computational methodologies and accurate material characterisation [16,24]. The mechanical behaviour of cellular parts may differ significantly across length scales as well [16,24,25,27]. The current models in the literature often face difficulties in accurately predicting patterns of deformation behaviour at numerous scales concurrently, and their accuracy could be restricted to particular scales due to computing constraints [16,29]. Additionally, natural cellular designs often have unique material characteristics such as nonlinearity, anisotropy, or viscoelasticity, which are not accurately captured by current deformation behaviour models of cellular structures in the literature [16,24–29]. The research area of bioinspired cellular parts is constantly changing with ongoing advancements and breakthroughs, such as in recently reported works on metamaterials [20–23], which have a behaviour that is dynamically dependent on external stimuli [30]. Therefore, it is necessary to understand the present trends in modelling of the structural behaviour of bioinspired cellular designs in order to identify possible extensions in the application of these behaviour models. Improving the capacity of deformation behaviour models related to bioinspired cellular parts could potentially open up new avenues for innovation in fields such as materials science, engineering, and biomechanics.

A recent broad review by Tuninetti et al. [31] provides an extensive state-of-the-art overview of biomimetic lattice structures, with a particular focus on design strategies, manufacturing routes, and application-driven performance under high stress, deformation, and energy absorption. In contrast to that work, the present review paper does not aim to survey lattice architectures or manufacturing technologies in breadth. Instead, it focuses specifically on the analytical modelling of deformation mechanisms in cellular structures, with particular emphasis on extending existing formulations for compressive response and proposing new analytical expressions to better describe load transfer and failure initiation in cellular or lattice structures.

The material in the ensuing sections documents extensions that are suggested here for the deformation behaviour of cellular parts, particularly their mechanism under compression loading. The first part of this material provides an overview of cellular designs highlighted in the recent literature. This is followed by a section that reviews the typically known two-stage stress–strain curve for cellular structures. This section additionally compares the two-stage stress–strain curve with a newly suggested curve, with a primary objective of extending the deformation mechanism already identified in the present-day literature. A subsequent section outlines analytical models available in the literature relating to the behaviour of cellular parts. In the same section, fresh models are introduced that more fully describe the behaviour of cellular structures. A further section highlights new strategies that could be implemented in integrating present-day deformation behaviour models, when optimising the design of cellular parts to enhance their mechanical properties. The last section in this paper highlights the expected challenges as well as prospects for the use of the new cellular behaviour models suggested here, in next-generation structural design for additive manufacturing (AM).

## 2. A Primer on Bioinspired Cellular or Lattice Designs

Bioinspired structural lattice parts are typically designed and manufactured based on complicated geometries of biological structures [4]. Organic structures that are typically mimicked primarily for different engineering uses have progressively evolved over

millions of years to attain noteworthy mechanical properties such as specific stiffness [7], specific energy absorption [15,18], specific strength [4,15], fracture toughness [12], customisable design features [16,17], and lightweight property [10–12,15–17,19,28]. Scientists and engineers aspire to generate new structures and materials featuring comparable or improved mechanical performance for numerous types of engineering uses by mimicking these organic designs [4,10–12,16,17,19,28]. Following is a primer on some useful structural cellular parts observed in nature and their corresponding biomimetic parts highlighted in a number of recent works [10–12,15–17,19,28,29].

Honeycomb structures, modelled after the hexagonal celled structure observed in beehives, are built up of a series of unit hexagonal cells structured in a repeating pattern [15]. This design and other similar designs of polygonal hollow structures including those built using triangles, rectangles, circles, pentagons, and heptagons, have good strength-to-weight ratios and are typically adopted in aerospace, automotive, and packaging industries [4,15]. Polygonal geometries can distribute loads evenly and their hollow structures do attain high strength-to-weight ratios with minimal use of material, thus making them well-suited for lightweight structural applications [15,17]. Bones are a natural composite material built using collagen fibres and calcium phosphate crystals. The hierarchical structure of a bone tissue, which consists of microscale collagen fibres reinforced with nanoscale mineral crystals, gives both strength and flexibility in design [2,4,7]. Engineers research the anatomy of bones to build lightweight and strong materials primarily for generating structural parts such as orthopaedic implants, and protective gear [11,27]. Wood tissues are other types of hierarchical biological materials, primarily built from cellulose fibres within a matrix of lignin and hemicellulose. Their cellular structures, which include elongated cells known as tracheids and specialised water-conducting cells in angiosperms, provide strength, flexibility in design, and toughness [7,32–34]. Wood-inspired materials are being built for use in architecture, home furnishings, and renewable energy uses [32–34]. The silk produced by spiders is a protein-based biological material recognised for its good strength, customisability in design, and toughness. Spiders generate silk fibres featuring a wide range of characteristics for many applications, including construction of webs, capture of prey, and building of shelter [35]. Researchers are investigating ways to mimic spider silk's mechanical properties for different engineering uses, including textiles, medical sutures, bulletproof vests, and biodegradable plastics [36–38]. Nacre material, often referred to as mother-of-pearl, is a colourful material that occurs in mollusc shells. It is built up of multiple layers of aragonite (a type of calcium carbonate) interwoven with organic proteins. Nacre has high toughness and resilience to fracture because of its hierarchical configuration, which aids in absorbing energies and withstanding the progression of cracks [39]. Engineers are investigating nacre for use in producing durable yet lightweight materials for armour, coatings, and medical implants [40,41]. Another example of biological cellular structures is the spines of cactus, which are hierarchical structures designed for collecting water and providing mechanical support. Their in-built conical shapes and surface microstructures allow for the effective absorption of water and its storage [42]. Researchers are conducting research into cactus-inspired structures for developing materials for capturing water in arid areas and improving the effectiveness of biomimetic surfaces [43–45]. The foregoing examples highlight the range of bioinspired structural cellular components and demonstrate their potential for use in a wide range of engineering industries. Scientists and engineers strive to build novel materials and structures that have improved performance and sustainability by borrowing from such natural designs. Table 1 documents a few biological structures selected in this paper, in addition to their corresponding biomimetic structures [15,46–57].

**Table 1.** A few selected biological cellular designs and their corresponding bioinspired parts in engineering uses [15,46–57].

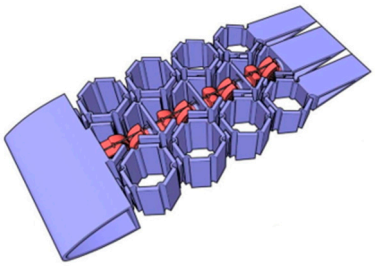
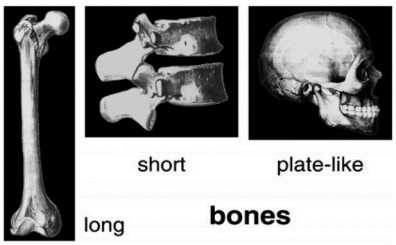
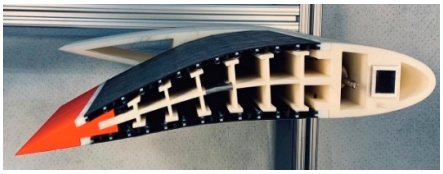
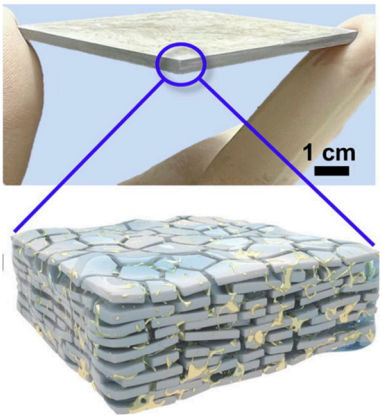
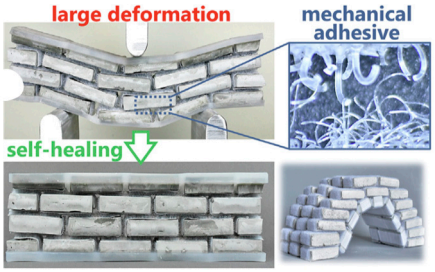
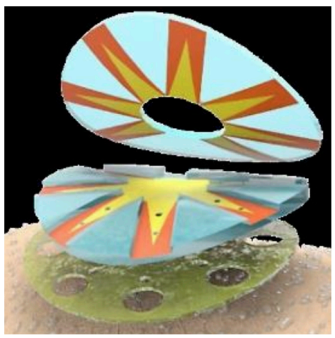
| Selected Biological Cellular Structures | Engineering Uses of Some Selected Biomimetic Structures |
| --- | --- |
|  (a) Honeycomb structure observed in beehives [46] |  Aircraft honeycomb wing structure with the integrated mechatronic nodes [47]  Non-pneumatic tyre-embedded hexagonal spokes [15] |
|   (b) Bone structures [49] |  Wing structure inspired by fish bones [50]  Bone-inspired chair [51] |

**Table 1.** *Cont.*

| Selected Biological Cellular Structures | Engineering Uses of Some Selected Biomimetic Structures |
| --- | --- |
|  (c) Nacre structure [52] |   Nacre-inspired conductive material [53]   Nacre-inspired structures with self-healing elastomeric, cementitious, or mechanical adhesives [54] |
|  (d) Cactus-spine [55] |  Cactus-spine-inspired sweat sensor [56]  Cactus-spine-inspired water collector [57] |

The ensuing discussion is on the recently reported research on bioinspired cellular parts shown in Table 1 [15,46–57], and the authors' suggestions to extend research, are introduced in each case, with respect to applications.

- Wang et al. [58] reviewed a suggested four-layer dielectric absorption honeycomb design that uses a genetic algorithm to produce incidence angle insensitive reflection loss in the 4–18 GHz frequency region. Their algorithm programme could be tailored towards the design of smart material-driven honeycomb-configured stealth inlets used in future propulsion systems. Moat et al. [59] conducted experimental and numerical studies on the mechanical properties of additive-produced honeycombs with shapes drawn from the 'hat' class of aperiodic tiling. They observed that by tailoring the tiling parameters, a customisable Poisson's ratio between the range of 0.45 and 0.006 is attainable. Investigating the influence of different materials on the mechanical properties of these honeycombs could identify material-specific behaviour and extend their engineering uses. Qin et al. [60] used numerical analysis and experimental testing to show the feasibility of the suggested node-locked multi-cell honeycomb design concept, in addition to investigating the influence of different design parameters on the resulting structures' capabilities to absorb energy. The new design strategy of a multicellular structure for absorbing energy was proven to be cost-efficient. Further research on the prospect of incorporating additional features into the multi-cell honeycomb architecture, such as thermal insulation, acoustic damping, or electromagnetic shielding, to build multifunctional structures with multiple uses.
- Audibert et al. [61] generated an algorithm that adopted a bio-inspired strategy based on the bone structure to optimise the design of mechanical parts. The suggested method was found to be useful based on experimental test results. Extending Audibert et al.'s algorithm through the incorporation of more biological principles or optimisation strategies. This could enhance its capacity to generate optimal designs for a broader range of mechanical parts and applications. Barba et al. [62] used powder bed fusion with a minimum strut thickness of 250 μm to achieve the lowest resolution possible with their technology for bone-inspired parts. Some lattice topologies that required careful attention to sensitive features were reported to be challenging to work with successfully from the outset. Design more effective process control and monitoring strategies for detecting and minimising manufacturing flaws such as porosity, warping, or distortion in bone-inspired lattice structures during printing. This could include incorporating in situ sensor technology or real-time feedback control systems to guarantee consistent quality of parts.
- Natural nacre typically exhibits a tensile strength of 80–135 MPa and a toughness of 1–3 MJ/m$^3$; Wang et al. [63] developed artificial nacre using alumina micro-platelets, graphene oxide nanosheets, and polyvinyl alcohol ($Al_2O_3$/GO-PVA). This artificial nacre outperformed natural material, achieving a strength of 143 $\pm$ 13 MPa and toughness of 9.2 $\pm$ 2.7 MJ/m$^3$. The authors credited the improved efficiency to the hierarchical structures comprising micro-platelets ($Al_2O_3$) and nanosheets of varying length scales. The generated films of $Al_2O_3$/GO-PVA had a tensile strength 2.8 times greater than $Al_2O_3$/PVA films and a toughness about 6 times higher than GO-PVA films, indicating that the three-component composite is advantageous for harmonising strength and toughness. Exploring new strategies for functionalising and modifying the surfaces of alumina micro-platelets and graphene oxide nanosheets to customise their interactions with the polyvinyl alcohol matrix and improve the general characteristics of the composite. This could entail using chemical treatments, surface coatings, or the inclusion of groups of functional parts that enhance compatibility and adhesion of the constituents, and strength of the final structures formulated. Finnemore et al. [64] produced artificial nacre through a layer-by-layer deposition technique in combination with a crystallisation step that mimics the mineral tablet-forming process in natural nacre. Nanomechanical analysis using nanoindentation showed identical deforma-

tion behaviour in artificial and organic nacre. Under loads that cause cracking and shear failure in monolithic calcite and aragonite, respectively, the manufactured nacre exhibited a pile-up behaviour and plastic deformation, which reduced fracturing. Generate multiscale modelling and simulation techniques for predicting the mechanical properties and structural performance of artificial nacre based on its microstructural characteristics and composition. This requires integrating features such as atomistic, mesoscale, and continuum-level models to capture in detail the complex interactions and mechanisms leading to deformation of the structure at different length/size and time scales.

- Li et al. [56] built a water collector with micro bionic branch spines and a customisable wettability feature, which was followed by manufacture of the composite material to be followed by post-processing. This built cactus-inspired structure was found to have a remarkable water collection performance. The spiny spine which had a sharp angle of 10° showed the greatest water-collecting capacity when compared to different tip angles (20°, 30°, 40°, and 50°). At the same time, superhydrophobic nanomaterials were sputter-coated onto the surface of the designed structure, and it was observed that the water-collecting capacity of the cactus-simulated thorn with a superhydrophobic coating was far greater than that of the 3D printed cactus-simulated thorn with no coating. Extended studies should be conducted towards enhancing the geometry and wettability of the miniature bionic branch spines to maximise their water collection capacity. This could include investigating a broader range of spine shapes, such as variations in length, curvature, and spacing, as well as different types of surface treatments or coatings that control wettability as well as improving the water collecting capacity. Wang et al. [65] integrated the water collection mechanisms of the cactus spine and Sarracenia plant to attain drop-by-drop capture and rapid water transfer. The peculiar trichome's multilayer microchannel structuring that was observed in the bioinspired hybrid structure allowed for a threefold faster water transfer as compared to the capacity of the cactus spines or spider silk. Examination of the prospect of using the bioinspired hybrid structure for multiple applications beyond water harvesting, including anti-fog coatings, self-cleaning surfaces, or microfluidic devices for biomedical diagnostics is proposed. For better performance and adaptability in different environments and industries, this would involve incorporating additional features or surface treatments to the structure.

Recent research [66–68] has revealed that energy absorption in cellular structures extends beyond the classical plateau and densification behaviour typically discussed. In particular, certain topologies such as Kelvin cell lattices exhibit significant hysteretic damping under cyclic or dynamic loading, a form of mechanical energy dissipation where the loading–unloading path encloses a non-zero area, indicating energy loss per cycle. This behaviour has been observed experimentally in polymeric lattice metamaterials fabricated via processes such as material extrusion and vat photopolymerisation, where hybrid or re-entrant architectures display enhanced tan $\delta$ and increased hysteresis work during cyclic compression tests, indicating effective vibration damping and energy dissipation mechanisms tied to geometry-driven frictional and viscoelastic effects rather than purely elastic responses. Similarly, studies on TPU and resin lattices have shown that Kelvin and related periodic structures can stabilise dynamic responses and accelerate vibrational attenuation compared to non-architectured parts, highlighting the influence of topology on damping characteristics [69].

Critically, recent work [70] on LPBF-fabricated Kelvin lattice metamaterials has demonstrated that such topology-driven hysteretic damping is not limited to polymeric systems but is also intrinsic to metallic architectured materials. An integrated experimental-

numerical framework was developed to characterise elastic–plastic hysteresis under cyclic loading, enabling accurate prediction of energy dissipation, stiffness degradation, and the evolution of damage with increasing load cycles. Unlike conventional analyses focused solely on plateau stress and densification, this framework explicitly captures rate-dependent plastic deformation and hysteresis loop formation, and further allows identification of the initial fracture point and subsequent failure progression within the lattice. These results reveal ultrahigh damping efficiencies in LPBF Kelvin lattices arising from controlled plasticity and microstructural interactions inherent to the unit-cell topology, which cannot be inferred from monotonic stress–strain responses alone.

In the metallic domain, lattice metamaterials, including those with Kelvin-like unit cells, are increasingly investigated for their combined energy absorption and damping performance, particularly under dynamic and cyclic loads enabled by laser powder bed fusion (LPBF). While most metallic lattice research still emphasises plateau energy absorption, several studies report that controlled deformation mechanisms and microstructural interactions contribute to rate-dependent dissipation and modifications to stress–strain hysteresis, beyond what simple static curves capture [71]. Incorporating experimentally validated hysteretic and damage-aware constitutive behaviour into deformation and optimisation models is therefore essential for accurately representing the full spectrum of energy dissipation mechanisms in high-performance lattice structures.

## 3. Stress–Strain Curves for Cellular or Lattice Structures

An overview of the known two-stage stress–strain curve for cellular structures is presented in this section, followed by a comparison of it with a newly suggested curve by the authors, aiming towards extending comprehension of the deformation mechanisms prevailing in such structures.

### *3.1. Two-Stage Stress–Strain Curve for Cellular or Lattice Designs*

During the first stage of deformation observed in the typical two stage stress–strain curve, cellular structures are represented as acting elastically, with a linear relationship between stress and strain. During this stage, the structure's cells are assumed to stretch or compress while remaining structurally intact. The slope of the stress–strain curve in this region is taken to represent the material's stiffness, also known as Young's modulus [65,72]. Following the first deformation, cellular structures often go into a plateau state with a relatively constant stress level despite rising strain. The plateau phase is caused by different kinds of mechanisms, including buckling, bending, and collapse of cell walls, which allow the material to withstand more deformation without significantly increasing stress. During this stage, the material could undergo significant plastic deformation while remaining under relatively constant stress, exhibiting a high level of energy absorption and structural resilience [72–74]. Figure 1 shows a typically adopted two stage stress–strain curve for cellular structures in engineering uses [72].

In its entirety, the open literature only discusses a two-stage deformation curve for cellular structures, which ranges from elastic behaviour characterised by a linear stress–strain response to the plateau phase, in which the material undergoes plastic deformation while maintaining close to constant stress. Comprehending these behaviours has implications when building and optimising cellular designs that meet particular performance-standards such as mechanical strength and energy absorption.

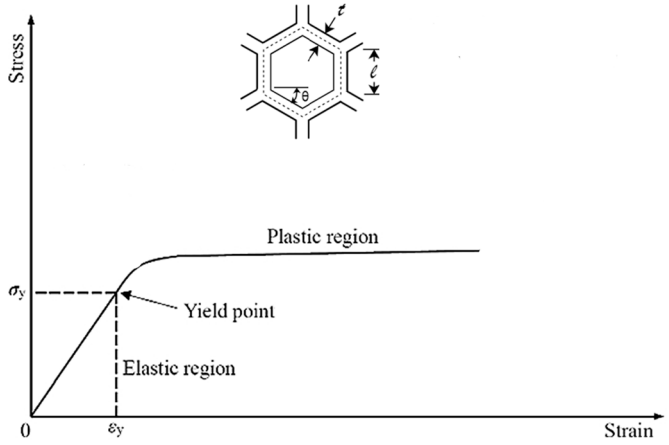



**Figure 1.** A typical two stage stress–strain curve for cellular designs [72].

### *3.2. A Novel Mechanism of Deformation Added to the Two-Stage Behaviour of Cellular or Lattice Designs*

Cellular structures, such as foams, honeycombs, and numerous types of lattice structures, have different mechanical properties due to their intricate internal designs. Though the stress–strain curve for cellular structures in the literature generally follows standard trends, such as elastic deformation followed by plastic deformation of the cellular materials [72], additional mechanisms unique to these structures are now presented here to better represent their deflection and deformation.

In a typical stress–strain curve, the elastic region depicts the range of elastic deformation, which means that the material returns to its original shape after the applied load is removed. Though the two-stage stress–strain curve provides useful insights into the deformation behaviour of cellular structures, the authors [75] did recently recommend consideration of the various deformation mechanisms prevailing during loading of cellular structures. To this end, it posed here that for cellular designs, there are two separate stages of elastic deformation that have not been reported in the available literature and which when considered lead to the four-stage stress strain curve shown in Figure 2.

The first stage identified represents buckling and bending deflection of the structure. The second stage includes the onset of densification causing elastic deformation of the material, combined with buckling, and bending deflection of the structure and thus its higher structural stiffness. The third stage represents sole elastic deformation of the material after full densification, which is the reason for it having a higher stiffness than the first two stages. It is important to note here that buckling does not precede elastic deformation; rather, buckling is itself an elastic instability that arises from the linear elastic response of a slender, load-bearing member. The sequence illustrated in Figure 2 is intended to describe the geometric evolution of a free-standing lattice strut under increasing load, where elastic deformation first manifests as bending and buckling of the unconstrained member, followed by contact with neighbouring struts. Once such contact occurs, the deformation behaviour transitions toward that of a more constrained or effectively solid structure, after which the response resembles the conventional elastic–plastic deformation observed in fully dense materials. Stage four is where plastic deformation of the fully densified structure occurs and thus a plateau is formed.

It is important to note here that the stiffness in the first three stages in Figure 2 will vary from material to material and structure to structure, while maintaining the observed increase in value from the first to the third stage. Moreover, the plateau denotes pure plastic deformation, which does not apply for metallic structures but rather strain hardening till an ultimate tensile stress and eventual drop in stress till failure that is known to prevail for metallics. Equation (28) in this paper and the supporting derivations leading to it followed

by the discussion beneath it give credence to the sequential mode of deformation failure proposed in this paragraph. Recent work by the authors on experimental quasi-static crushing of hexagonal Ti6Al4V (ELI) lattice structures demonstrated collapse primarily through bending and buckling, Poisson's ratio lateral expansion of cells, and sliding horizontally and along directions inclined and to the direction of application of load. Loading in this case stopped before the establishment of full contact of adjacent members of the lattice structure due to limitations in the travel of the loading jaws of the testing frame [76].

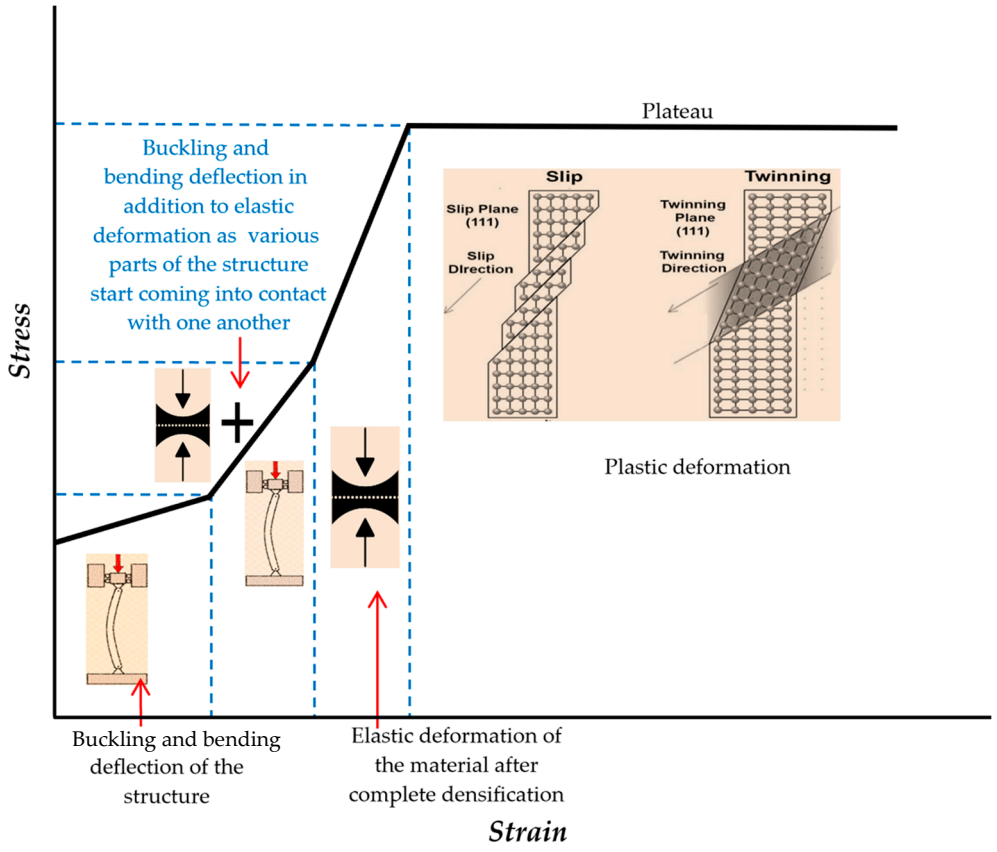



**Figure 2.** A proposed four-stage stress–strain curve for cellular designs.

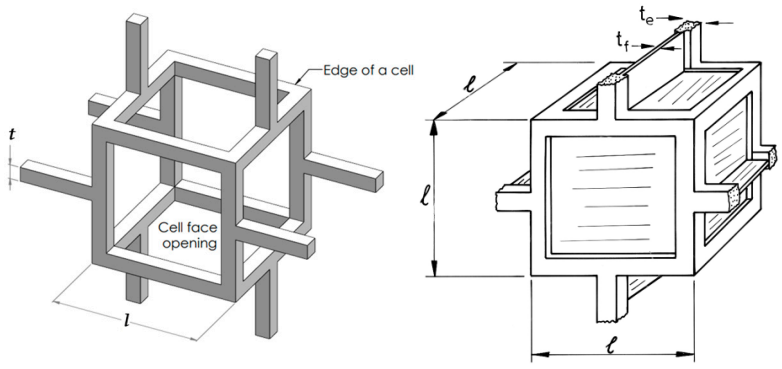
Stage two of the curve shown in Figure 2 represents an intermediate phase between the first phase of elastic structural deformation comprising buckling and bending deflection and the third phase of elastic deformation of the material. This intermediate step avails a stress versus strain curve that provides a more accurate representation of the deformation process occurring in cellular structures, based on a fuller recognition of the underlying mechanisms that govern the material and structural behaviour of cellular structures.

## 4. Analytical Modelling of Ductile Failure of Cellular Structural Members Based on Both the Tresca and Von Mises Criterion for Ductile Materials

Cellular designs, which are typically built up of repeated unit cells, exhibit complex deformation behaviour due to their peculiar architecture. Different models have been developed that describe this behaviour, according to various cellular structures and uses [77,78]. This section of the paper examines the Gibson and Ashby models in particular, which are used for different investigations on the deformation behaviour of cellular structures found in the literature. The first model, put forth by Ashby & Gibson [72,79], relates the mechanical properties of foams to their relative densities. It is based on the concept of

scaling principles as well as on empirical studies of numerous types of foams. The fundamental mechanical properties of elastic modulus, yield strength, and energy absorption as functions of relative density are captured by the model. The first Gibson and Ashby model has been improved on and updated over the years in an effort to improve its accuracy and usefulness. These improvements take account of aspects such as size, shape, or thickness of the cell wall. The Gibson and Ashby model has been extensively adopted in the design and optimisation of cellular materials for a wide range of engineering applications, including, impact absorption, thermal insulation, lightweight structures, and biomedical implants [72–75,77–79]. The model aids engineers and materials scientists in choosing or designing foams with particular characteristics matched to their intended application by predicting the mechanical behaviour of foams based on their relative densities.

The Gibson and Ashby models provide a framework for analysing the mechanical behaviour of cellular structures centred on their geometry and material properties. Their models for predicting the behaviour of cellular structures are typically built based on two geometries, namely the open and closed cellular shapes [79]. Open cellular structures are three-dimensional polyhedral open-cell designs constructed from foamy material and interconnected by controlled hollow-like struts. Their orientation space is often determined by perforated holes and random cell wall configurations. This particular type of cellular structure is recognised by its solid edge shape [79,80]. In contrast, the closed cellular designs are replicas of the open-cell shape with added solid faces, resulting in cells being enclosed [79]. Figure 3a,b show unit cell geometrical representations of an open and a closed cellular structure, respectively [72,75,79].




(**a**) (**b**)

**Figure 3.** Gibson and Ashby models for a (**a**) unit open cellular shape and (**b**) unit closed cellular shape [72,75,79].

Both open and closed cellular structures have advantages as well as drawbacks, and the option between the two is often influenced by the application's particular requirements, including mechanical performance, weight considerations, fluid permeability, and manufacturing constraints [72–75,78]. The behaviour models of these two types of cellular structures are limited to elastic deformation.

Open cellular designs at first exhibit linear elastic behaviour when loaded with small deformations, primarily governed by stretching and bending of the cell walls and struts. The structures return to their original shape once the applied load is removed, as long as the deformation remains within the elastic limit of the material. However, open cellular structures are also liable to buckling under compressive loads, particularly for slender struts or cells [72,79]. Figure 4 shows Gibson and Ashby models built for describing the bending and buckling behaviour of open cellular structures [79].

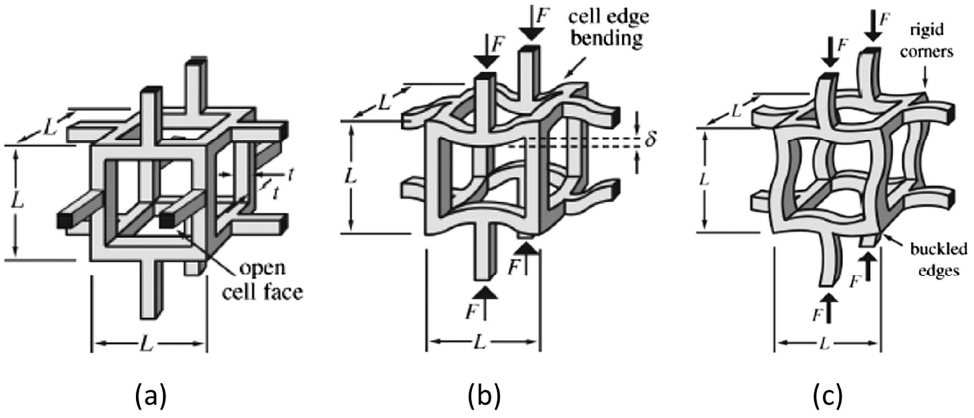



**Figure 4.** Open unit cell shape that has (**a**) no deformation, (**b**) buckling deformation, and (**c**) bending deformation [79].

Designing for critical loading conditions is a paramount concept in the field of engineering that must be considered for safety, reliability, and optimal performance in a wide range of applications, including civil infrastructure, automotive, aeronautical, and medical engineering [80]. Presently, only critical loading conditions in the transverse and axial directions are considered in the deformation behaviour models for cellular structures discussed here. The geometries for cellular designs are normally built up of beams or ribs. Therefore, theories of beams are often adopted for developing their corresponding behaviour models [72,75,77–79]. Figure 5 shows the transverse loading of an open cellular structure, represented by the mid-span concentrated transverse loading of a beam fixed at both ends. This load case is often thought of as the critical transverse loading scenario for a cellular structure [81].

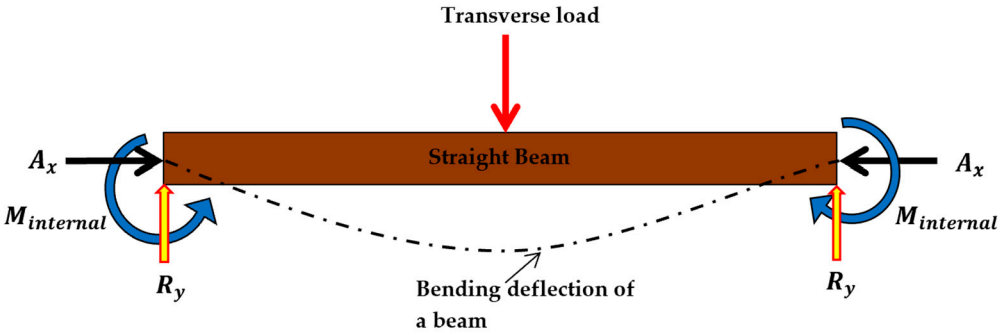



**Figure 5.** A mid-span concentrated transverse loading of a beam fixed at both ends, similar to one used in building cellular structures [79].

For simplicity, the ensuing analysis is based on a beam with a rectangular cross-section with sides of breadth $b$ and depth $h$, both of which are equal to one another and may be represented by the symbol $t$. Figure 6 shows the cross-section of the beam, and the associated parameters used.

The cross-sectional parameters of a rectangular beam with the cross-section shown in Figure 6 lead to the second moment of area $I$ presented as shown in Equation (1).

$$I = \frac{bh^3}{12} = \frac{t^4}{12} \quad (1)$$

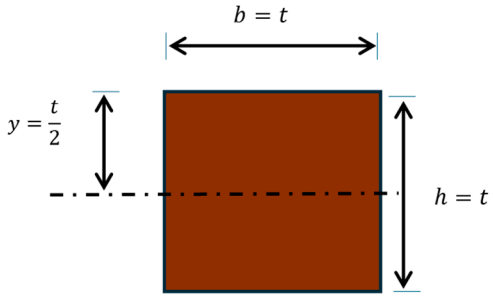



**Figure 6.** Cross-section of rectangular beam and corresponding parameters adopted here.

Substituting this equation into the expression for maximum transverse deflection of a central point loaded beam that is fixed at both ends [81], such as the one shown in Figure 5, leads to the following equation.

$$y_{max} = \frac{\epsilon}{R} = \frac{FL^3}{192EI} = \frac{FL^3}{16Et^4} \tag{2}$$

The symbols $\epsilon$, $R$, $F$, $L$, and $E$ in the foregoing equation represent the normal strain, radius of curvature of the beam, applied load, length of the beam, and elastic modulus of the beam's material, respectively. The expression in Equation (2) highlights the fact that the maximum transverse deflection $y_{max}$ of ribs/beams for a cellular structure is inversely proportional to both the modulus of elasticity $E$ of the chosen material of the structure and is also inversely proportional to parameter $t$ raised to power 4. These two relationships are from the equation seen to be linear and no-linear, respectively. This implies that the cellular structure with a greater value of parameter $t$ will be able to withstand higher transverse loads as compared to one with a smaller value. This is consistent with the observations made in reference [81]. The maximum bending stress $\sigma_{bmax}$ generated in the cell walls or ribs of a transversely loaded cellular structure is determined using the following general equation for bending [72,79,81].

$$\sigma_{b_{max}} = \frac{M_{max}}{I} y \tag{3}$$

The symbol $M_{max}$ in Equation (3) represents the maximum bending moment experienced under a transverse load $F$ applied onto the ribs building up a cellular structure. For arbitrary distances $a$ and $b$ from the left and right fixed support points of a horizontal beam to the point of application of a transverse point load, respectively, the maximum bending moment is equal to, and reduces for mid-span concentrated loading to, in this order [79,81].

$$M_{max} = \frac{2Fa^2b^2}{L^2} \qquad M_{max} = \frac{FL}{8} \qquad \text{for } x = \frac{L}{2} \tag{4}$$

The symbol $L$ in the preceding equation represents the length of the transversely loaded beam or rib of the cellular structure. Substituting Equation (1) and the right one of Equation (4), into Equation (3) gives rise to the following expression:

$$\sigma_{max} = \frac{3FL}{2t^4} y \tag{5}$$

From the numerous studies conducted on the behaviour of loaded beam structures [72,79,81], it is known that $\sigma_{bmax}$ occurs on the outermost fibres of the ribs or beams building up cellular designs, in which fibres the symbol y = $t/2$. Therefore, Equation (5) can be simplified to

$$\sigma_{bmax} = \frac{3FL}{4t^3} \tag{6}$$

Clearly, from Equation (6), $\sigma_{bmax}$ is inversely proportional to parameter $t$ raised to power 3. The relationship is nonlinear, which is consistent with the observations made in references [71–75,78,79]. The maximum bending stress $\sigma_{bmax}$, is also seen from the equation to increase with increasing $L/t^3$ ratio.

In addition to the bending stresses, shear stresses also play a significant part in the structural stability of lattice structures. Understanding how shear stresses are distributed within the connecting members assists in ensuring that they remain within the elastic limit of the material to prevent premature failure. The shear stress induced in the rectangular cross-section shown in Figure 6 for the transverse concentrated load $F$ of the beam shown in Figure 5 is described by Equation (7) [81].

$$\tau_{xy} = V\frac{A\overline{y}}{bI} = \frac{3F}{t^4}\left[\left(\frac{t}{2}\right)^2 - {y_1}^2\right] \tag{7}$$

The symbol $V$ in Equation (7) represents the transverse shear force induced in each rib of the chosen cellular/lattice design. Parameter $V$ for the centrally loaded, fixed beam is known from standard engineering texts to be equal to $F/2$. The maximum transverse shear stress is known to occur at the centroidal axis where the parameter $y_1$ is equal to zero, thus reducing Equation (7) to [81]:

$$\tau_{xy}\big|_{max} = \frac{3F}{4t^2} \tag{8}$$

The maximum transverse shear stress is seen from Equation (8) to be inversely related to parameter $t$ raised to the power 2. As with Equations (2) and (6), this relationship is nonlinear. Thus, small changes in parameter $t$ will result in significant differences in the maximum transverse shear stress. From the expressions presented in Equations (6) and (8), the ratio between the maximum bending stress and the maximum transverse shear stress is derived as

$$\frac{\sigma_{bmax}}{\tau_{xy}\big|_{max}} = 2\left(\frac{L}{t}\right) \tag{9}$$

Since the ratio $L/t$ for cellular structures is always greater than unity, the ratio $\sigma_{bmax}/\tau_{xy}\,|_{max}$ will always be greater than one. This, combined with the knowledge that shear yield stress is known to be equal to half the direct yield stress [81], suggests that failure for such cellular structures is $L/t$ more times probable to occur due to induced bending stresses than from induced shear stresses, for a concentrated load applied at midspan. This is similar to what has been reported in references [72,81]. The $L/t$ ratio for cellular structures is typically equal to at least 5, to ensure sufficient structural stability. This helps maintain the material's ability to resist bending deformation under loads [72,79].

For the case of longitudinal loading of the ribs or beam structures used to build cellular parts, Gibson and Ashby [79] reported that either direct or buckling deformation are likely to occur. In its simplest form the direct deformation of a unit rib or beam used to build cellular designs can be represented by the expression for direct stress given here as Equation (10).

$$\sigma_{x(a)} = -\frac{F}{A} = -\frac{F}{t^2} \tag{10}$$

The symbol $A$ here represents the cross-sectional area $bh = t^2$, whereas the minus $(-)$ sign represents compression loading. The direct stresses induced in the beam are caused by internal opposition to the externally imposed axial load $F$, causing compressive or tensile behaviour in the beam [81]. The direct deformation $\delta$ caused by direct axial loading of the beam here is represented as shown in Equation (11).

$$\delta = \frac{PL}{EA} = \frac{PL}{Et^2} \tag{11}$$

The symbol $E$ in the foregoing equation represents the modulus of elasticity of the chosen material. Buckling deformation can occur as well in these structurally thin members also referred to as struts under direct axial loads. This deformation behaviour is determined by the stiffness, boundary constraints, and the value of the load that is imposed on the struts. Figure 7 shows the buckling behaviour of a strut in an open cellular configuration with fixed ends. The critical load in this case results in buckling along the effective length $L_E$, as highlighted in the Figure [81].

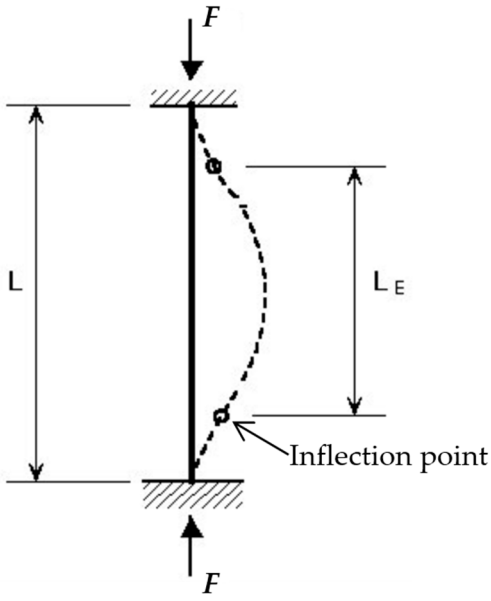



**Figure 7.** A strut fixed at the ends under direct axial loading [81].

Based on the general Euler buckling theory, Gibson and Ashby [72,79] derived the critical buckling load $F_e$ as presented in Equation (12).

$$F_e = \frac{\pi^2 EI}{L_e^2} = \frac{\pi^2 Ehb^3}{12L_e^2} = \frac{\pi^2 Et^4}{12L_e^2} \tag{12}$$

The critical buckling stress $\sigma_e$ of a strut is determined from Equation (12) as

$$\sigma_e = -\frac{F_e}{A} = -\frac{\pi^2 Et^2}{12L_e^2} \tag{13}$$

A comparison of the critical buckling stress, maximum bending stress, and maximum transverse shear stress is carried out in the next section to make a statement of their relative significance for the same applied point load $F$.

The elastic deformation behaviour of closed cellular structures is arguably more complicated as compared to that of open cellular structures. For closed cellular structures, cases of internal pressure combined with the transverse as well as direct loads in the vertices must be considered [72,75,77]. The deformation of closed cellular structures not only involves the effects of these last two types of loads but also stretching of cell wall membranes under internal pressure. The pressure generated inside closed cellular structures is caused by the compression of fluids enclosed in cavities found in the cellular cells and the corresponding shortening and lengthening of the cell walls [79,80]. Figure 8 shows a hexagonal closed cellular structure, in addition to the two orientations in which the cellular structure extends under applied internal or external pressure [79].

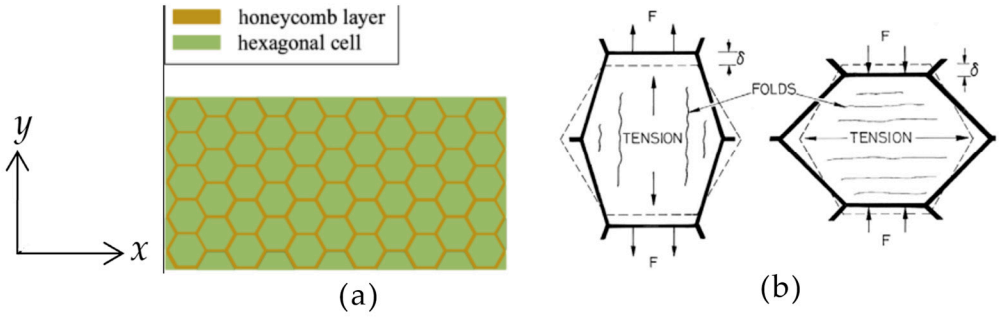



**Figure 8.** A hexagonal closed cellular structure, (**a**) the geometry before deformation, and (**b**) the stretching deformation in the x- and y-directions [79].

Given that pressure loads act over finite areas of membranes, the load is considered to be uniformly distributed across the membrane and, therefore, the effects of stress concentration are often disregarded. Depending on the magnitude of the ratio $L/t$, a loaded cell wall could be regarded as a thick or thin plate, with fixed-end constraints on all six edges [72,79–83]. Cellular structures typically occur as thin plates, which effectively minimises the usage of material, while interconnection of the walls provides additional restrain on each wall, thus maintaining the structures' overall load-bearing capacity [1–3,72,79,84].

There are numerous different topologies used to form cellular or lattice structures, including circular, square and rectangular grids, triangular lattices, Kagome lattices, re-entrant (auxetic) cells, diamond and octet truss lattices, gyroid and other triply periodic minimal surface (TPMS) architectures [2–5,78,79,83,84]. The hexagonal topology has been studied here rather than these alternatives due to its widespread use, well-established analytical frameworks, and favourable balance between stiffness, strength, and energy absorption. Moreover, the modelling, optimisation, and scaling approaches adopted for the hexagonal lattice are topology-agnostic in formulation and can be systematically extended to other lattice architectures with appropriate geometric and boundary condition modifications.

The classical theory of plates, specifically the Love Kirchhoff's theory with its eight assumptions [84,85], can be used to determine the deflection and stresses induced in them by any applied loads. The case of bending moments ($M_x$ and $M_y$) acting on the edges of a plate is represented as shown in Figure 9, which for a thin plate leads to the generation of a two-dimensional stress state [85].

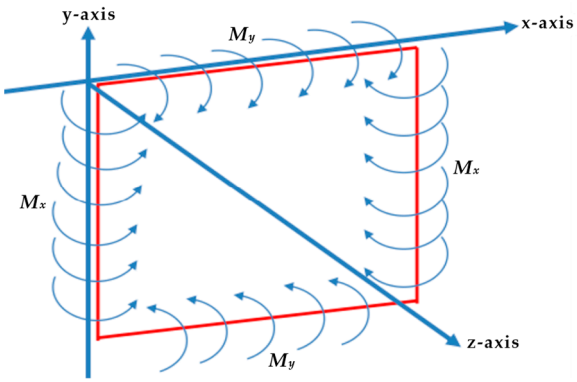



**Figure 9.** A two-dimensional representation of a thin plate under x- and y-directional bending moments [85].

It is clear from Figure 9 that the induced bending moments due to externally applied loads cause out-of-plane bending deflections of the thin plates in cellular structures. Such bending deflections are counteracted by opposing bending moments induced by pressure generated inside closed cellular structures, which is caused by the compression of fluids

contained in the cavities found in them. As a consequence, closed cellular architecture deforms not just at the vertices connecting unit cells, but also as a result of in-plane stretching of the thin walls used to encapsulate fluids inside their cavities. Equations (14) and (15) define the relationships between the induced bending moments in the $x$- and $y$-direction, respectively, and the in-plane mutually orthogonal radii of curvature, with parameter $D$ defined as shown in Equation (16) [85].

$$M_x = D\left[\frac{1}{R_x} + \frac{\nu}{R_y}\right] \tag{14}$$

$$M_y = D\left[\frac{1}{R_y} + \frac{\nu}{R_x}\right] \tag{15}$$

$$D = \frac{Et^3}{12(1-v^2)} \tag{16}$$

The symbols $D$, $v$, $t$, and $R$ represent the flexural stiffness, Poisson's ratio, thickness of the unit cell, and radii of curvature of the loaded thin plate, respectively. The direct stresses in a thin plate are inversely related to the radii of curvature and are directly proportional to the distance from the neutral plane, through its thickness [85,86]. It has been shown in standard engineering textbooks that with some manipulation, the foregoing first two equations give rise to Equations (17) and (18) for the direct in plane-stresses induced in such a plate [81,85]

$$\sigma_x = \frac{12M_x z}{t^3} \tag{17}$$

$$\sigma_y = \frac{12M_y z}{t^3} \tag{18}$$

### *4.1. Proposed Model Combining Direct, Buckling and Bending Deformation of Cellular or Lattice Structures*

Integrating direct, buckling, and bending deformation behaviours in a new model proposed here for lattice structures is expected to result in better predictions of their mechanical deformation behaviour. The proposed model is based on the free body diagram shown in Figure 10 showing two connected ribs of an open lattice structure under combined direct and bending loads.

To determine which one of direct, buckling, and bending deformations arising from the load scenario shown in Figure 10 is critical, the direct and shear yield stresses of the material must be combined in a single function together with the direct, shear and bending loads arising from the applied load in the structure. This approach provides a better means of accessing failure of lattice structures as opposed to the prevalent approach that carries out the analysis load by load and member by member [60,62,72]. The maximum bending moment and bending stress at yield in the horizontal member in Figure 10 will occur at midspan and are given by Equations (5) and (6), reproduced here as Equations (19) and (20) for ease of reference [64,81]:

$$M_{max} = \frac{FL}{8} \tag{19}$$

$$\sigma_{b|max} = \frac{3FL}{4t^3} \tag{20}$$

To determine the maximum allowed bending load $F_{b\,|\,max}$, at yield the applied load ($F$) is made the subject in Equation (6) at this maximum allowed value, thus

$$F_{b|max} = \frac{4\sigma_y t^3}{3L} \tag{21}$$

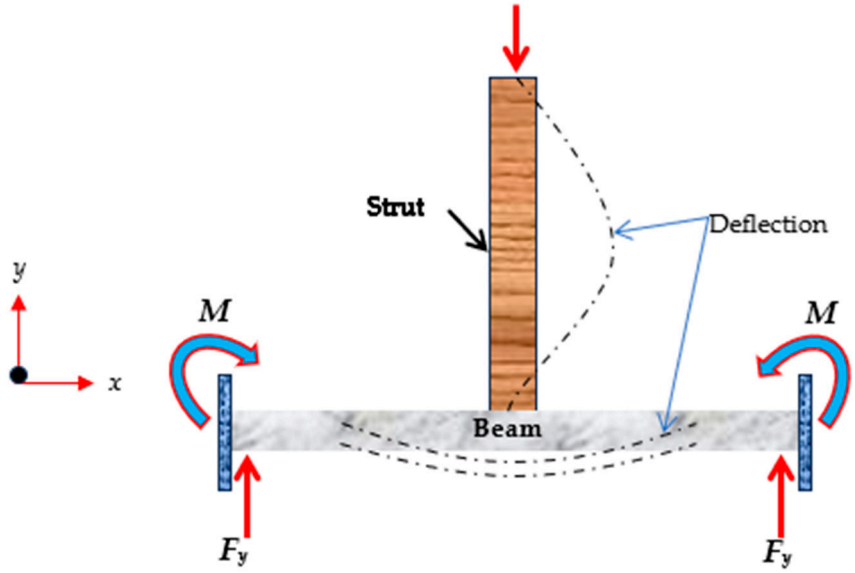



**Figure 10.** Combined direct, buckling, and bending deformation of ribs used to build open lattice structures.

In the case of buckling of the vertical rib in Figure 10, the critical load presented here as $F_{e\,|max}$ is equated to the term for the first mode of buckling in the Euler equation, thus [81]

$$F_{e|max} = \frac{\pi^2 EI}{{L_e}^2} = \frac{4\pi^2 EI}{L^2} = \frac{\pi^2 Et^4}{3L^2} \tag{22}$$

The effective length is assigned for fixed struts. The buckling stress $\sigma_{e\,|max}$ (not yield stress) at this critical buckling load is obtained from the ratio of this critical load and the cross-sectional area of the strut $A = (t^2)$ thus giving rise to the relationship:

$$F_{e\,|max} = \sigma_{e\,|max}\,\mathrm{A} = \sigma_{e\,|max} t^2 \tag{23}$$

Substituting this expression into Equation (22) and making the direct stress at this critical load the subject leads to the equation

$$\sigma_{e\,|max} = \frac{\pi^2 Et^2}{3L^2} \tag{24}$$

The compressive maximum allowed direct stress $\sigma_y$ is determined as follows:

$$\sigma_{d|max} = \frac{F}{A} = \frac{F}{t^2} \tag{25}$$

Therefore, the critical direct load is equal to

$$F_d|_{max} = \sigma_y t^2 \tag{26}$$

The applied loads for critical direct and buckling as well as bending stresses induced in the vertical strut as well as horizontal strut of the lattice structure are given by the ratio of Equations (26) and (22), as well as (21), respectively, thus

$$F_{d|_{max}} : F_{e|max} : F_{b|max} = \sigma_y t^2 : \frac{\pi^2 Et^4}{3L^2} : \frac{4\sigma_y t^3}{3L} \tag{27}$$

This relationship may be simplified to

$$F_{d|_{max}} : F_{e|max} : F_{b|max} = 1 : \frac{\pi^2 E t^2}{3L^2 \sigma_y} : \frac{4t}{3L} \tag{28}$$

Substituting typical values of the parameters $E$, $t$ and $L$ for materials used to produce lattice structures of thin walls shows that the largest, second largest, and lowest values of these loads are for direct, bending, and buckling loads, respectively. From the foregoing analysis, the most critical mode of failure for the applied load shown in Figure 10 is buckling followed by bending and lastly direct. However, this analysis is limited, as it considers each of these modes of failure separately. The best practice is to consider the direct, bending, transverse shear and buckling all together, as is performed in the next section.

### *4.2. Suggestions on the Application of Tresca and Von Mises Failure Criteria to the Deformation Behaviour of Cellular or Lattice Designs*

The Tresca and von Mises failure criterions find application in engineering for predicting the failure of materials under complex stress conditions [80]. These criterions are generally used to predict failure of components made of homogenous materials [83–85] and can also be applied to lattice structures. To the best of the authors' knowledge, there are limited analytical models available in the literature describing the use of these failure criterions on lattice structures. The Tresca criterion, also referred to as the maximum shear stress theory, suggests that a material fails when its maximum shear stress exceeds a critical threshold [83]. The Tresca criterion can be used for lattice structures by considering the stress condition at critical points within the structure, such as interfaces of cells or locations with high stress concentrations. The criterion can be used to determine the start of yielding or plastic deformation in lattice parts, particularly in areas where shear loads are predominant. The von Mises criterion, referred to as the equivalent stress or distortion energy criterion, contends that a material fails when its equivalent von Mises stress exceeds a critical value [83–86]. This criterion is commonly employed for ductile materials and is particularly useful in predicting failure under combined loading conditions [83–86]. For lattice structures, both the Tresca and von Mises criterions can be used to determine the equivalent failure stress based on the prevailing principal stresses at specific spots on the structures. Both criterions can be used in cases where tensile, compressive, and shear stresses occur simultaneously.

To provide proof of the value of these two suggested criterions for failure in lattice structures, the authors here present the analysis of a beam structure similar to the one used as a building block for lattice parts under loads in order to determine the limiting loads. The present work examines the failure of a beam structure under the already discussed transverse and direct loads using a two-dimensional (2D) principal stress example. This is performed because beam structures used for building cellular designs are often viewed as plane stress problems [72,78,79,81,83]. Plane stress occurs in cases where the out-of-plane direction is so thin that it carries no stress in that direction [81,83]. Combining the equation for principal stresses and the Tresca criterion for a plane gives rise Equation (29) [81].

$$\tau_Y = \frac{\sigma_1 - \sigma_2}{2} = \frac{\sqrt{(\sigma_x - \sigma_y)^2 + 4\tau_{xy}^2}}{2} \tag{29}$$

For the type of loading shown in Figure 10, the direct stress $\sigma_y$, acting on the horizontal member is zero, which transforms Equation (29) to

$$\tau_Y = \frac{\sigma_1 - \sigma_2}{2} = \frac{\sqrt{\sigma_x^2 + 4\tau_{xy}^2}}{2} \tag{30}$$

Substituting the expressions for the bending and transverse shear stresses, Equations (6) and (8), respectively, for the load case shown in Figure 10, into Equation (30) in terms of the applied load $F$ gives rise to the following equation for the stress at which shear failure occurs:

$$2\tau_Y = \sqrt{\left(\frac{3FL}{4t^3}\right)^2 + 4\left(\frac{3F}{4t^2}\right)^2} \tag{31}$$

By making the applied vertical load ($F$) the subject of a known shear failure stress ($\tau_Y$) of the material for the horizontal lattice member, a critical value of the applied vertical load can be calculated, thus

$$F_{hor}|_{critical} = \frac{8\tau_Y t^3}{3\sqrt{L^2 + 4t^2}} \tag{32}$$

Buckling stress in Figure 10 will arise in the vertical member for loads higher than or equal to the buckling load. A horizontal deflection of the member will occur concurrently with a bending stress that is defined by a bending moment that is a product of the difference between the applied load and the buckling load, and the bending deflection of the member. The arising bending stress and direct stress are, respectively, equal to

$$\sigma_b = \frac{3(F - F_e)L}{4t^3} \quad and \quad \sigma_d = \frac{F}{t^2}$$

Therefore, the total direct stress induced in this member is equal to the sum of bending longitudinal stress and direct stress, thus

$$\sigma = \sigma_d + \sigma_b = \frac{3(F - F_e)L}{4t^3} + \frac{F}{t^2} = \frac{F(3L + 4t) - 3F_eL}{4t^3} \tag{33}$$

Noting that there is no shear load that is imposed on the vertical beam implies that $\tau_{xy} = 0$, thus Equation (30) reduces to

$$\tau_Y = \frac{\sigma_1 - \sigma_2}{2} = \frac{\sqrt{\sigma_x^2 + 4 \times 0^2}}{2} = \frac{\sigma_x}{2} \tag{34}$$

Substituting Equation (33) into Equation (34) leads to

$$\tau_Y = \frac{\sqrt{\left(\frac{F(3L+4t)-3F_eL}{4t^3}\right)^2}}{2}$$

If the ratio of the applied to the buckling load is represented by the symbol ($r$), and making the applied load ($F$) the subject of the preceding equation, allows the critical value of this load to be represented as follows:

$$F_{ver}|_{critical} = \frac{8\tau_Y t^3 r}{(3Lr + 4tr - 3L)} \tag{35}$$

The critical values of the applied forces ($F_{hor}$ and $F_{ver}$), calculated from Equations (32) and (35), respectively, enable determination of which one of the two members is more critical based on which critical force is lower for the load case shown in Figure 10, using the Tresca criterion.

For the horizontal member in Figure 10, the von Mises criterion for two-dimensions yields the following equation for the case where the stress ($\sigma_y$) is equal to zero:

$$\sigma_Y = \sqrt{\sigma_x^2 + 3\tau_{xy}^2} \tag{36}$$

Substituting Equations (6) and (8) for bending and transverse shear stresses in the horizontal member in Figure 10, respectively, into the first and second terms in Equation (36) in this order, gives rise to

$$\sigma_Y = \sqrt{\left(\frac{3FL}{4t^3}\right)^2 + 3\left(\frac{3F}{4t^2}\right)^2} \tag{37}$$

Invoking the known relationship between direct and shear yield stresses under uniaxial loading allows this equation to be rewritten as

$$2\tau_Y = \sqrt{\left(\frac{3FL}{4t^3}\right)^2 + 3\left(\frac{3F}{4t^2}\right)^2} \tag{38}$$

Making the applied load the subject of this equation generates the following expression for the critical applied load with reference to the horizontal member in Figure 10:

$$F_{hor}|_{critical} = \frac{8\tau_Y t^3}{3\sqrt{L^2 + 3t^2}} \tag{39}$$

Application of the von Mises criterion to the stresses induced in the vertical member in Figure 10 follows the same reasoning as in the preceding case of the Tresca criterion. Thus, it is observed again that buckling stress in Figure 10 will arise in the vertical member for loads higher than or equal to the buckling load. Again, it is noted that horizontal deflection of the vertical member brings about a bending stress that is defined by a bending moment that is a product of the difference between the applied load and the buckling load, and the bending deflection of the member. Therefore, as previously noted, the arising bending stress and direct stress are, respectively, equal to

$$\sigma_b = \frac{3(F - F_e)L}{4t^3} \quad and \quad \sigma_d = \frac{F}{t^2}$$

Therefore, as noted before, the total direct stress induced in this member is equal to the sum of bending longitudinal stress and direct stress, thus

$$\sigma_x = \sigma_d + \sigma_b = \frac{3(F - F_e)L}{4t^3} + \frac{F}{t^2} = \frac{F(3L + 4t) - 3F_eL}{4t^3} \tag{40}$$

Again, noting that there is no shear load that is imposed on the vertical beam implies that $\tau_{xy} = 0$, thus Equation (36) reduces to

$$\tau_Y = \frac{\sigma_1 - \sigma_2}{2} = \frac{\sqrt{\sigma_x^2}}{2} \tag{41}$$

Substituting Equation (40) into Equation (41) leads to the expression

$$\tau_Y = \frac{\sqrt{\left(\frac{F(3L+4t)-3F_eL}{4t^3}\right)^2}}{2}$$

As previously done, if the ratio of the applied to the buckling load is represented by the symbol ($r$), and making the applied load ($F$) the subject of the preceding equation, allows the critical value of this load to be represented as follows:

$$F_{ver}|_{critical} = \frac{8\tau_Y t^3 r}{(3Lr + 4tr - 3L)} \tag{42}$$

The critical values of the applied forces ($F_{hor}$ and $F_{ver}$), calculated from Equations (39) and (42), allow identification of the more critical member for the load case shown in Figure 10, based on which critical force is lower using the von Mises criterion.

Examination of Equations (35) and (42) shows that regardless of whether the vertical member is evaluated under the Tresca or von Mises yield criterion, its behaviour in the event of buckling remains the same, as the two equations are the same.

While the analytical models presented in Equations (32)–(42) provide tractable predictions of critical forces and deformation behaviour for conventional hexagonal lattice structures, it is important to acknowledge their limited applicability to hybrid or multifunctional lattice architectures, where multiple unit-cell typologies interact in complex ways. Recent studies, including Khan et al. [87], emphasise the need for multi-scale, topology-optimised, or numerical modelling frameworks to capture the performance of such hybrid lattices, particularly when targeting multifunctionality or simultaneous optimisation of stiffness, strength, and energy absorption. In contrast, the present analytical approach is most suitable for single-typology, regular lattices with uniform strut geometries, and serves as a first-order tool for rapid design exploration rather than a comprehensive predictive framework for all modern metamaterial designs. Future extensions should integrate multi-scale or topology-optimised strategies to address these limitations while retaining the insights offered by analytical formulations.

Figure 11 shows the relationships between the critical load and the thickness parameter $t$ for constant values of the length of lattice members of 7 mm. The curves present the critical horizontal and vertical forces corresponding to both the Tresca and von Mises failure criteria, thus enabling evaluation of cellular or lattice members under different loading conditions and failure criteria.

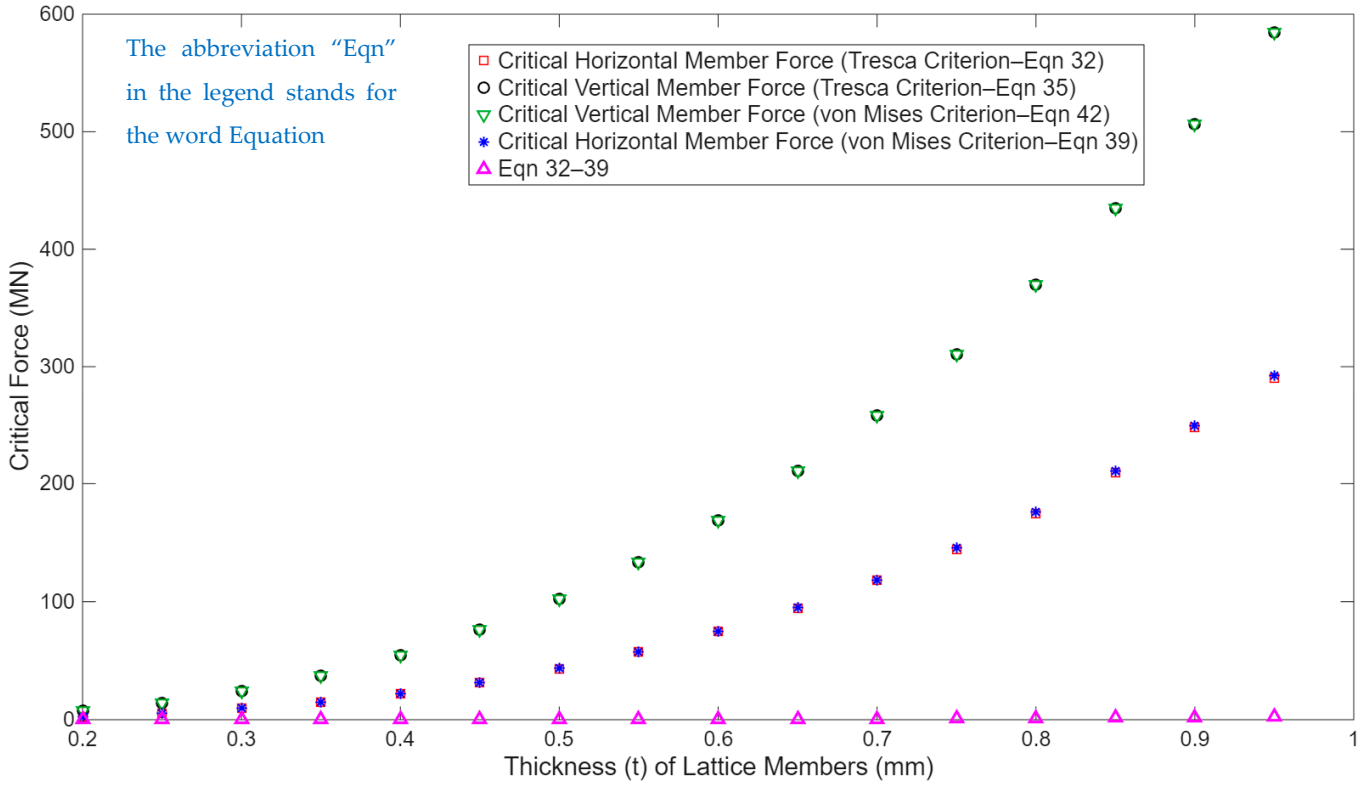



**Figure 11.** Curve plots for critical force against the thickness parameter ($t$) of lattice members.

The curves in Figure 11 show the variation in critical forces at a constant value of the length of lattice members of 7.0 mm. The figure shows the critical forces (the maximum

forces a lattice member can withstand before failure or buckling) predicted from the analytical expressions developed here to be nonlinearly dependent on the thickness of members of lattice structures. It is clear in this figure that, as $t$ increases from a value of 0.2 to 1.0 mm, all the curves of critical load in the figure increase continuously at an increasing rate. This trend is consistent with bending-dominated, buckling-dominated or mixed-mode loading whereby the increase in critical loads with increasing thickness is a function of $t^3$ for all these three types of loads, as is evident in Equations (32), (35), (39) and (42). The green and hatched red curves are coincident as so are the yellow and black hatched curves. This implies that the difference in the critical forces derived from either one of the two failure-criterion only occurs between the vertical and horizontal member but not for any one of the two members alone. The green and hatched red curves of the Tresca criterion-based and von Mises criterion-based vertical member critical forces are seen to be higher and to increase much faster than the curves of Tresca criterion-based and von Mises criterion-based horizontal member critical forces. This implies that vertical struts are the primary load-bearing elements in the compression of lattice structures. The brown curve (Equations (39)–(32)) hugging the zero horizontal line is such because the difference between the two analytical expressions stays comparatively much smaller, with absolute values between thicknesses of lattice members of 0.2–0.95 mm, being in the range 0.001–0.906 MN, respectively. This large changes in the magnitudes of the critical forces seen in the top four curves in Figure 11 demonstrate that micro-geometry tuning of thickness is a powerful tool for tailoring the mechanical response of cellular or lattice structures.

The curves in Figure 12 illustrate the relationship between the predicted critical forces and the geometric parameter of length ($L$) for constant values of lattice member thickness of 0.575 mm of lattice members.

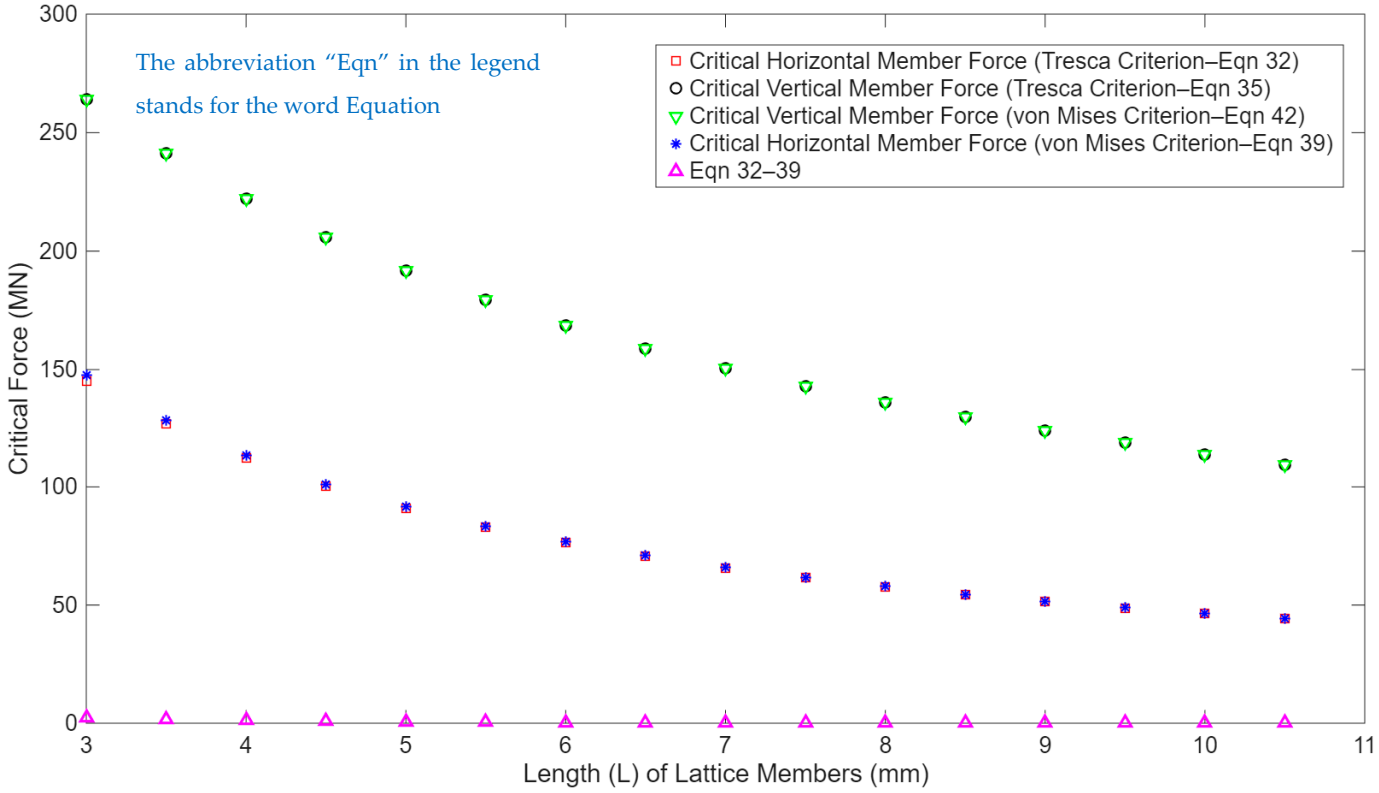



**Figure 12.** Curve plots for critical force against length ($L$) parameter of lattice members.

In this figure, as was the case in Figure 11, the Tresca criterion-based and von Mises criterion-based vertical member critical forces are seen to be greater than the curves of

Tresca criterion-based and von Mises criterion-based horizontal member critical forces. Therefore, the same conclusion is arrived at as from the curves in Figure 11, that vertical struts are the primary load-bearing elements in the compression of lattice structures. The critical forces in this case decrease at a decreasing rate with increasing length of the lattice members in contrast to the case for thickness of lattice members in Figure 11. This is not all together surprising as increasing the length of lattice members at constant values of their thickness increases their slenderness ratio and, therefore, reduces their load-bearing capacity. In this graph as was the case in Figure 11, the difference in the critical forces for the horizontal member (plotted here as a brown curve) is comparatively much smaller than the absolute values for lengths of the lattice members between 3 and 10.5 mm, ranging between 0.217 and 0.076 MN, respectively.

The curves in Figure 13 illustrate the relationship between the predicted critical forces and the geometric parameter of slenderness ratio ($t/L$) of lattice members for values of lattice member thickness and length varying between 0.2 and 0.95 mm and 3 and 10.5 mm, the same range for each used in plotting the curves for Figures 11 and 12, respectively.

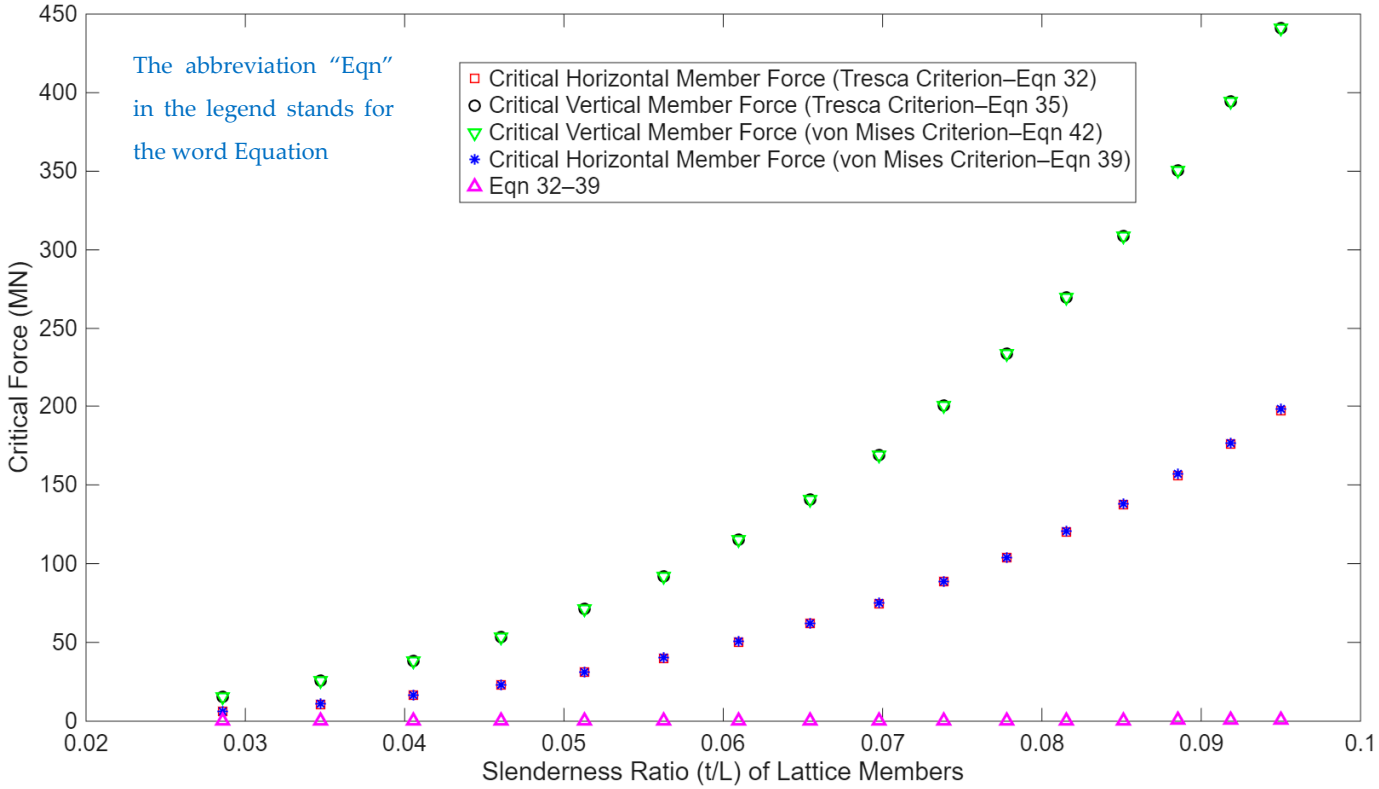



**Figure 13.** Curve plots for critical force against the slenderness ratio ($t/L$) of lattice members.

The characteristics of and conclusions arising from the curves shown in Figure 13 are the same as those of the curves shown in Figure 11, with the difference that the top four curves in Figure 13 are significantly steeper that the top four curves in Figure 11. The increase in critical force with increasing slenderness ratio ($t/L$) of the vertical lattice member seen in Figure 13 is significant as the slenderness ratio is the primary determinant of the stability of vertical frame members. As the slenderness ratio of vertical members increases, their radii of gyration ($k = \sqrt{I/A} = t/2\sqrt{3}$, for members with rectagular cross $-$ sections) and buckling resistance also increase, thus leading to exponential growth in their load carrying capacity [79,81]. Similar exponential growth with increasing thickness of lattice members was also evident in Figure 11 and emphasises the fact that even small increases in the thickness of lattice members lead to disproportionately large gains in their load-bearing

capacity. This is critical for the optimisation of lattice designs, where small penalties due to higher weights from slightly thicker members can yield large benefits of strength.

The analytical formulations developed in this study (Equations (32)–(42)) describe the critical force response of hexagonal lattice unit cells under idealised loading conditions and are intended to provide first-order insight into the governing deformation trends rather than exact failure predictions. While the trends presented in Figures 11–13 are derived analytically, the validity of the underlying assumptions and predicted response has been previously examined by the authors through detailed finite element analysis (FEA) of additively manufactured polygonal and hexagonal lattice structures [88]. In this earlier work by the authors, comprehensive static and stability-driven FEA was performed on hexagonal and polygonal lattice structures manufactured from DMLS Ti6Al4V (ELI), considering bending-dominated, buckling-dominated, and direct loading scenarios. That study demonstrated strong agreement between analytically predicted deformation modes and numerically observed stress distributions, buckling patterns, and load–displacement trends at the unit-cell level. In particular, the transition between bending-dominated and buckling-dominated behaviour observed numerically is consistent with the trends predicted by the critical force expressions presented here and illustrated in Figures 11–13. The analytical model developed here is, therefore, a reduced-order representation of deformation behaviour that has already been numerically verified under comparable geometric and loading conditions. Performing additional FEA within the scope of this paper would be redundant given that the primary objective of the present study is to establish closed-form analytical relationships that enable rapid parametric exploration and design insight.

Though the Tresca and von Mises yield criteria provide useful first-order insight in this study, they are classical continuum-based models with well-established limitations when applied to architectured lattice and metamaterial systems. The two criteria yield different predictions, with Tresca being more conservative due to its dependence on maximum shear stress, while von Mises is governed by the second deviatoric stress invariant and produces smoother yield surfaces. Both assume material isotropy and homogeneity, which restricts their direct applicability to lattice architectures that exhibit effective orthotropic or anisotropic behaviour arising from geometric periodicity and strut orientation, even when the parent material is nominally isotropic. For additively manufactured Ti6Al4V in particular, experimentally observed anisotropy has been shown to be strongly dependent on length scale and processing history, as demonstrated by systematic multi-scale experimental correlations reported in [89]. This distinction is essential to avoid conflating intrinsic material anisotropy with geometry-induced anisotropy in lattice systems.

Moreover, classical yield criteria are derived under idealised elastic–perfectly plastic assumptions and are incapable of capturing dominant failure mechanisms in low-relative-density lattices, including strut buckling, fracture, and instability-driven collapse. In architectured metamaterials, directional stiffness and strength are frequently dictated by topology rather than material behaviour alone, as rigorously demonstrated in [90]. This confirms that anisotropy in lattice systems is often an intentional, topology-driven design outcome rather than a violation of continuum material assumptions.

Neither the Tresca nor von Mises criteria account for strain hardening, damage evolution, hydrostatic stress sensitivity, or anisotropic plastic flow, all of which are known to govern failure in additively manufactured Ti6Al4V. Advanced constitutive investigations, such as an assessment of damage and anisotropic plasticity models to predict Ti6Al4V behaviour [91], explicitly demonstrate the inability of isotropic yield criteria to predict damage initiation and fracture evolution in this alloy system. Accordingly, in the present work, these criteria are deliberately employed only to identify the onset of plastic yielding at the

strut level and to establish conservative comparative bounds across lattice configurations, not to predict post-yield response or ultimate failure.

The limitations of isotropic yield criteria in porous AM lattices, where fracture is governed by void nucleation, growth, and coalescence, are therefore explicitly acknowledged. Incorporation of micromechanical damage models or continuum damage mechanics formulations would be required to capture damage accumulation and its coupling with plastic deformation. While such approaches would significantly enhance predictive fidelity, their integration falls outside the scope of the present analytical framework and is reserved for future multi-scale and numerical extensions.

The analytical models developed herein further assume isotropic material behaviour. This assumption was intentionally adopted as a first-order modelling choice to preserve analytical tractability and to establish baseline deformation relationships. Extension to orthotropic or fully anisotropic constitutive descriptions was not pursued, as it would introduce substantial complexity without proportionate gains in predictive accuracy for well-manufactured components. Fully densified LPBF Ti6Al4V (ELI) specimens produced in our laboratory between 2015 and the present have consistently exhibited minimal anisotropy, largely confined to the build direction, with near-isotropic in-plane properties [92–94]. This observation aligns with experimental findings by Moletsane et al. [92] and Van Zyl et al. [93], which show that mechanical directionality in LPBF Ti6Al4V is primarily governed by build strategy and process parameters rather than intrinsic material behaviour.

Consistent with the broader literature, including multi-scale experimental studies [94–97], pronounced anisotropy in additively manufactured Ti6Al4V is typically associated with suboptimal process control, inadequate thermal management, or insufficient post-processing rather than being an inherent feature of the AM process. When appropriate parameter optimisation and heat treatment are applied, near-isotropic mechanical behaviour is routinely achieved. Consequently, anisotropy in LPBF Ti6Al4V should be regarded as a manufacturing-quality indicator rather than a governing material constraint in lattice design.

Based on this understanding, the analytical models presented in this work are expected to remain valid for high-quality AM-produced lattice structures, with any minor build-direction effects introducing only second-order deviations in predicted response. Rather than embedding anisotropy directly into lattice design models, the findings reinforce the position that manufacturing process control and parameter optimisation are the primary means of mitigating directional behaviour, ensuring that isotropic analytical models remain a reasonable and practical approximation for design-stage analysis.

## 5. Prospective Routes for Optimising Lattice or Cellular Designs Using Models for Their Deformation Behaviour

Optimising lattice structures includes tailoring their shape and distribution of materials to attain particular performance targets, including strength, stiffness, or absorption of energy. Deformation behaviour models are of significance in this optimisation strategy as these models give insight into how these structures respond to mechanical loads. This section looks at some such prospective strategies for optimising lattice structures using deformation behaviour models.

Finite element analysis (FEA) is a well-established and effective numerical modelling tool for predicting the behaviour of complicated structures under a broad range of loading situations [98–102]. Engineers can further develop the method for analysing the effectiveness of lattice structures and iteratively optimising their design by incorporating advanced or new deformation behaviour models into FEA packages. The FEA tool can predict the distribution of stress, deformation, and modes of failure [103]. In turn, this allows designers

and engineers to customise the topology and distribution of materials in lattice structures for the best performance possible. In addition, tools capable of leveraging computational fluid dynamics (CFD) and discrete element modelling (DEM) could be used in conjunction with deformation behaviour models to mimic the behaviour of complicated lattice structures under different operating conditions [23]. These strategies allow engineers to examine the effectiveness of lattice structures in numerous types of loading conditions and to optimise their design accordingly.

Incorporating strut-level deformation and failure models into finite element analyses enables more accurate predictions of global stiffness, yield onset, and collapse behaviour of lattice structures than homogenised continuum approaches. This hypothesis can be evaluated by systematically comparing homogenised lattice models with strut-resolved simulations and corresponding experimental results under uniaxial, shear, and multiaxial loading conditions. Key metrics for comparison include effective stiffness, peak load capacity, deformation localisation, and dominant failure mechanisms. Establishing benchmark datasets across a range of relative densities and lattice topologies allows the modelling error and predictive fidelity of each approach to be quantified.

Topology algorithms for optimisation assist with the re-distribution of materials within a particular design space to achieve optimal objectives of structural performance [104]. Engineers can generate lattice designs with customised mechanical properties by incorporating advanced or cutting-edge deformation behaviour models into topology optimisation tools. Deformation behaviour models inform the optimisation process by providing insight into how changes in geometry or distribution of materials influence structural performance [105]. These algorithms, coupled with the deformation behaviour models, primarily aid in the re-distribution of materials within a particular design space to meet the objectives of minimising stress concentrations, weight, or/and maximising stiffness while adhering to set design constraints. In addition, advanced deformation behaviour models could allow for the simultaneous investigation of numerous performance targets, such as increasing stiffness while reducing weight and ensuring structural integrity under various loading conditions [104,105]. Multi-objective optimisation approaches, such as genetic algorithms or Pareto optimisation, can be used to develop trade-off solutions that balance competing design objectives [106–108].

Topology optimisation frameworks informed by deformation behaviour models can generate lattice architectures with lower stress concentrations and superior stiffness-to-weight ratios than geometry-only optimisation approaches. This is achieved by explicitly embedding yield criteria, instability limits, or post-yield deformation measures within the optimisation process, rather than treating mechanical response as a downstream check. The resulting designs can then be benchmarked against conventionally optimised lattices using metrics such as maximum von Mises stress, compliance, mass, and failure load. Finally, selected Pareto-optimal candidates should be manufactured and mechanically tested to validate numerical predictions and to quantitatively assess the associated performance trade-offs.

Developing accurate constitutive models for the materials used in lattice structures is crucial for predicting their deformation behaviour. Deformation behaviour models, such as stress–strain curves, yield criteria, and strain-hardening behaviours, are used in material models that account for a structure's nonlinear response to loading [109]. Advanced material models, such as nonlinear elasticity, plasticity, and viscoelasticity, represent the complicated mechanical response of materials to changing loading conditions [109–111]. Incorporating these material models into deformation behaviour models could allow for more accurate predictions of structural performance and failure mechanisms. Furthermore, such deformation behaviour models are useful in determining the most suitable

material for lattice structures based on mechanical characteristics and performance requirements [109–113]. Engineers could identify materials with the best balance between strength, stiffness, and weight for a given engineering application by modelling their deformation responses under particular loading conditions. This informed material selection procedure could result in more optimised designs with better properties.

Strut-level constitutive models that explicitly account for nonlinear elasticity, plasticity, and strain hardening provide a more faithful representation of lattice post-yield behaviour and failure mechanisms. This premise can be directly tested by calibrating material models for additively manufactured lattices and systematically comparing predicted and experimentally measured stress–strain responses, deformation modes, and collapse mechanisms. Building on this, material-topology performance maps can be developed to link constitutive behaviour to optimal lattice architectures for prescribed loading scenarios.

Lattice structures typically show complex deformation behaviour across various length scales. Multiscale modelling strategies marry deformation behaviour models at multiple levels, from microstructural characteristics to the overall structure, to better describe the material's hierarchical behaviour [112,113]. This could be useful for accurately predicting deformation mechanisms such as plasticity, buckling, and fracture, as well as the optimisation of lattice structures at both the macroscopic and microscopic levels, while also considering material heterogeneity and microstructural features that influence performance.

Multiscale deformation models that explicitly link microstructural behaviour to the macroscopic lattice response enable more reliable prediction and optimisation across multiple length scales. This is achieved by coupling strut-level or microstructural models with unit-cell and full-structure simulations, and validating the resulting predictions against experimental observations of buckling, plastic hinge formation, and fracture. Such an approach allows the systematic quantification of how microstructural features and geometric hierarchy govern macroscopic lattice performance and failure.

Machine learning techniques are useful for analysing the large data sets generated by deformation behaviour models or experimental tests of lattice structures [114–116]. Data-driven strategies may provide insight into relationships between design parameters, material characteristics, and structural performance, leading to more effective optimisation strategies. Engineers can use machine learning techniques to accelerate the design process and explore design spaces that could prove challenging to analyse using traditional optimisation strategies. Moreover, deformation behaviour models can be integrated into manufacturing simulations to improve the manufacturability of lattice structures [113–116]. Engineers can design lattice structures that are both optimised for performance and manufacturable by considering manufacturing process constraints and material deposition behaviour in AM technologies.

Machine learning models trained on deformation behaviour data can accelerate lattice optimisation and uncover non-intuitive design–performance relationships beyond the reach of traditional methods. This approach can be evaluated by comparing machine learning-assisted optimisation with classical numerical techniques in terms of computational cost, prediction accuracy, and the ability to explore high-dimensional design spaces. Furthermore, integrating deformation behaviour models with manufacturing process simulations ensures that optimised lattice designs remain feasible within additive manufacturing constraints.

In its entirety, coupling deformation behaviour models and optimisation strategies allow for the efficient design of lightweight, high-performance lattice structures for a wide range of mechanical applications, spanning aerospace, automotive, biomedical, and structural engineering fields.

## 6. Anticipated Drawbacks and New Insights in Adapting Models for the Deformation Behaviour of Cellular or Lattice Structures Towards Advanced Structural Design for Additive Manufacturing

Adapting cellular behaviour models in upgrading structural design for AM provides both possibilities and challenges as is now discussed in this section of the paper.

The drawbacks include the following. Cellular structures often feature complicated structures with intricate lattice configurations or unit cells. Modelling these geometries accurately in numerical models can prove costly and difficult to generate, particularly for large-scale structures. This is because high-fidelity computational modelling of cellular structures in AM requires significant processing resources and time. Modelling complicated lattice designs with accurate material behaviour and loading conditions can take a long time, rendering such models not recommended for rapid design iterations or optimisation studies. Complicated geometries can additionally present challenges throughout the AM process with regard to material deposition, which may result in difficulties during the layer-by-layer fabrication or post-processing.

Current studies [31,117–120] address this challenge through unit-cell homogenisation, reduced-order models, beam-based strut idealisations, and selective local refinement strategies. Multiscale and sub-modelling techniques are increasingly used to limit full-resolution modelling to critical regions. While these approaches significantly reduce computational cost, they often sacrifice local accuracy, particularly in predicting strut-level plasticity, buckling, and failure localisation. Homogenised models, in particular, struggle to capture anisotropy induced by lattice topology and loading direction. There remains a clear need for hybrid modelling frameworks that dynamically balance computational efficiency and local fidelity, especially for optimisation-driven AM workflows where rapid iteration is essential.

Reduced-order or surrogate deformation behaviour models can achieve comparable accuracy to high-fidelity strut-resolved simulations at a fraction of the computational cost. Benchmark full-resolution lattice models against homogenised, reduced-order, or machine learning-assisted surrogate models using accuracy-cost trade-off metrics such as the error versus runtime, across increasing lattice complexity and scale.

Cellular behaviour models use accurate material parameters and behaviour models for predicting the structure's mechanical response. However, determining the material properties of AM-produced parts, particularly those with complex interior geometries, can be difficult. Variability in material properties caused by factors such as building direction, deposition patterns, porosity, layer adhesion, and thermal gradients or heat-affected zones can all have an impact on modelling accuracy. Failure to account for these factors could result in discrepancies between predicted and actual structural performance.

Researchers have introduced anisotropic material models, statistical descriptions of property variability, and experimentally calibrated constitutive laws tailored to specific AM processes and materials [121–124]. Most existing models remain process- or material-specific, limiting their generalisability. Furthermore, experimental characterisation of internal lattice struts remains challenging, leading to uncertainty in parameter calibration. Future deformation behaviour models must explicitly incorporate process–structure–property relationships, rather than relying on nominal bulk material properties, to improve predictive reliability across AM platforms.

Incorporating AM process-dependent material parameters into cellular behaviour models significantly reduces discrepancies between predicted and experimentally measured lattice response. The goal of developing constitutive models parameterised by build orientation, scan strategy, and thermal gradients, and validating them against mechanical tests of AM lattices produced under controlled variations should be pursued.

The seamless integration of cellular behaviour models into the AM design optimisation workflow brings both possibilities and drawbacks. Given that these models could provide insights into material behaviour at the microstructural level, turning this information into useful design parameters, requires the use of effective optimisation strategies and software tools. Bridging the gap between material modelling and design optimisation is crucial for realising the full capabilities of cellular behaviour models in AM. When designing cellular structures for AM, process-specific constraints such as minimum part sizes, overhang angles, and support requirements must be taken into consideration. Adapting cellular behaviour models to account for these constraints while optimising structural performance can be often challenging, requiring trade-offs between design complexity, manufacturability, and performance.

Topology optimisation, generative design, and multi-objective optimisation methods have been combined with simplified deformation metrics such as compliance or stress constraints [125,126]. Some studies have begun incorporating yield and instability criteria [126,127]. Despite progress, most optimisation studies rely on simplified mechanical indicators and rarely integrate full post-yield or failure behaviour. Manufacturing constraints are often treated as secondary filters rather than embedded directly into the optimisation process. There is a research gap in deformation-aware optimisation frameworks that simultaneously consider mechanical performance, manufacturability, and process constraints in a unified manner.

Optimisation frameworks that embed cellular behaviour models together with AM process constraints produce designs with superior manufacturability–performance balance compared to unconstrained optimisation. Explicitly integrating constraints such as minimum feature size, overhang limits, and supporting requirements into deformation-informed optimisation and quantifying performance loss versus manufacturability gains should be done.

Though cellular structures provide advantages in terms of lightweighting and material efficiency, optimising these structures for particular uses is still challenging. To generate optimal designs, researchers must navigate a large design space, which could require effective optimisation strategies and a significant amount of processing time. In addition, cellular behaviour models designed to work with particular AM technologies or materials could prove limited in scalability and ability to be generalised across multiple manufacturing conditions. Adapting these models to different manufacturing conditions, material compositions, and geometries while maintaining accuracy as well as effectiveness is a significant challenge. Developing adaptable models that can account for a variety of AM applications is a significant area of research.

Parametric modelling, dimensional analysis, and relative density-based scaling laws have been proposed to improve generalisability across lattice families [11,128]. While these methods improve portability, they often fail under complex loading conditions or for hierarchical and graded lattices, where deformation mechanisms deviate from idealised assumptions. Developing adaptable deformation models that remain valid across materials, scales, and AM processes remains a key open challenge for the field.

Cellular behaviour models formulated using non-dimensional parameters such as the relative density, slenderness, and normalised stress exhibit improved transferability across AM technologies. Model performance across multiple AM platforms and materials should be tested using normalised metrics to assess robustness and scalability.

In spite of advances in computational modelling, experimental validation is still imperative for guaranteeing the reliability and predictive accuracy of cellular behaviour models in AM. However, gathering experimental data for AM-produced structures can be difficult, particularly with regard to new or customised designs. It is still challenging

to accurately correlate numerical results with experimental findings. Moreover, running iterative tests to validate and develop such models can be time-consuming and resource heavy. Collaboration among researchers, industry partners, and AM practitioners is crucial for gathering results from experiments, confirming models, and driving forward progress.

Studies increasingly combine in situ monitoring, digital image correlation, X-ray computed tomography, and mechanical testing to validate numerical predictions [129–131]. Despite these advances, strong discrepancies often persist between numerical predictions and experimental outcomes, particularly for failure and post-collapse behaviour. Large-scale, standardised datasets are still lacking. Closer collaboration between academia and industry is required to establish benchmark datasets and validation protocols that improve model credibility and adoption.

Strategically designed experiments focusing on dominant deformation and failure modes are sufficient to calibrate and validate cellular behaviour models. Minimal yet representative experimental datasets targeting buckling, yielding, and fracture regimes, should be established and validation confidence versus testing effort quantified.

Even though these are expected shortcomings, the pursuit of upgraded structural design through cellular behaviour models in AM offers some new insights and prospects that are now discussed.

The latest insights and prospects include the following. Cellular behaviour models provide details regarding the most effective topology of structures for assigned performance requirements. Designers and engineers can investigate new and highly effective structure configurations that are physically challenging to manufacture via traditional methods by using advanced optimisation methods such as generative design algorithms. Furthermore, cellular structures built from advanced models could include higher performance characteristics such as improved strength-to-weight ratios, enhanced absorption of energy, and customised mechanical properties. This could result in the generation of new designs that are not feasible using conventional methods.

Generative and deformation-informed optimisation can identify lattice topologies with superior strength-to-weight and energy absorption compared to classical unit-cell families. Optimised lattices should be compared against benchmark topologies such as the hexagonal, octet, and TPMS, using standardised mechanical tests.

Additive manufacturing allows for the fabrication of complicated shapes and heterogeneous distributions of materials. Cellular behaviour models can use this capacity to customise material properties inside a structure to improve performance under various loading conditions. Cellular structures built using advanced models could result in multifunctional features, integrating structural integrity with additional functions such as thermal insulation, acoustic damping, and fluid flow control. This opens up new avenues for the integration of various functionalities into a single component or structure. Furthermore, using cellular architectures optimised by advanced modelling strategies, AM could minimise wastage of materials and the attendant consumption of resources while increasing the effectiveness of structures. This supports sustainability goals by encouraging resource efficiency and lowering environmental impact.

Cellular architectures optimised using coupled deformation-physics models outperform single-function lattices in multifunctional applications. Coupled mechanical-thermal-fluid simulations should be developed and experimentally multifunctional lattice performance validated.

By using multi-scale modelling approaches, engineers can accurately model the hierarchical structure of cellular materials, from microstructure to macroscopic behaviour. This comprehensive perspective allows for a better understanding of how local material characteristics influence overall structural performance, resulting in more accurate predic-

tions and optimised designs. In addition, advances in sensor technology allow for real-time monitoring of AM processes as well as in situ control of critical parameters. Coupling cellular behaviour models with these monitoring systems allows adaptive manufacturing strategies, in which the structural design could be tailored in real-time to guarantee consistent quality and performance.

Multiscale deformation models provide more accurate predictions of failure initiation and progression than single-scale models. Microstructure, strut-level response, and global behaviour should be linked, and prediction improvement across scales quantified.

Cellular architecture inherently provides material efficiency benefits, which correspond with sustainability objectives. Engineers can optimise cellular designs not only for performance but also for a lower environmental imprint, ultimately supporting sustainable manufacturing technologies. Moreover, the iterative nature of additive production allows rapid prototyping and design iteration. Cellular behaviour models aid this procedure by allowing engineers to quickly generate and analyse various design iterations, resulting in faster innovation cycles and reduced time-to-market for new products.

Coupling in situ monitoring with cellular behaviour models enables real-time adjustment of AM parameters to maintain structural performance. Integrating sensor feedback into deformation models and demonstrating closed-loop control in AM fabrication of lattice structures should be done.

As AM technologies advance, there is an emerging need for standardised methods for confirming and certifying AM-produced parts. Cellular behaviour models could play a significant part in this process by providing predictive capabilities that assist in validating the structural integrity and performance of AM parts, opening avenues for broader usage in crucial engineering applications.

Deformation-based predictive models can reduce material usage while satisfying certification requirements for safety-critical AM components. Developing certification-oriented modelling frameworks linking predicted deformation limits to regulatory acceptance criteria should be done.

In summary, though integrating cellular behaviour models in advanced structural design for AM poses challenges, it additionally presents unprecedented opportunities for innovation and optimisation. By resolving anticipated drawbacks and embracing fresh insights, engineers could realise AM's full potential for designing lightweight, high-performance structures tailored for particular engineering applications.

It is clear from the discussion in this section that additive manufacturing processes impose distinct geometric, material, and process-induced constraints that directly influence the mechanical response of cellular and lattice structures. As a result, deformation behaviour models developed for lattice optimisation cannot be considered process-agnostic, even when identical unit-cell topologies are employed. Key fabrication limits, such as minimum feature size, surface quality, build-induced anisotropy, and residual stress, govern both the attainable lattice geometry and the dominant deformation and failure mechanisms. Table 2 summarises the principal additive manufacturing processes used for cellular structures and explicitly links their fabrication limits to the corresponding implications for deformation behaviour modelling, highlighting the need for process-aware constitutive and structural models in design for additive manufacturing workflows [11,132–138].

**Table 2.** Comparison of additive manufacturing processes for cellular/lattice structures and their implications for deformation behaviour modelling [11,132–138].

| AM Process | Typical Materials | Fabrication Limits for Cellular Structures | Process-Induced Characteristics | Implications for Deformation Behaviour Modelling |
|---|---|---|---|---|
| Stereolithography (SLA) [11,132,133] | Photopolymer resins | • Minimum strut diameter limited by resin curing and light scattering<br>• Enclosed lattices require resin drainage<br>• Support removal constraints | • High geometric fidelity<br>• Smooth surface finish<br>• Brittle or quasi-brittle material response | • Linear elasticity valid only at low strains<br>• Yield criteria may be inappropriate; fracture-based or damage models preferred<br>• Buckling and brittle fracture dominate failure |
| Fused Deposition Modelling (FDM) [134,135] | Thermoplastics (PLA, ABS, PETG, Nylon) | • Minimum strut size limited by nozzle diameter<br>• Overhang angle and filament sagging<br>• Limited inter-layer bonding | • Strong anisotropy<br>• Layer-wise porosity and voids<br>• Reduced strength in build direction | • Orthotropic or anisotropic material models required<br>• Isotropic yield criteria (Tresca, von Mises) are insufficient<br>• Inter-layer failure and shear-dominated deformation must be captured |
| PolyJet [136] | Photopolymers, multi-material systems | • Support material entrapment in fine lattices<br>• Limited thermal resistance<br>• Material ageing effects | • High resolution and smooth surfaces<br>• Spatially varying material properties<br>• Viscoelastic behaviour | • Viscoelastic or time-dependent constitutive models required<br>• Spatially heterogeneous material modelling needed<br>• Homogenised models may mask local property gradients |
| Laser Powder Bed Fusion (LPBF) [137,138] | Metals (Ti6Al4V, Al alloys, steels) | • Minimum strut size limited by laser spot and powder size<br>• Unfused powder removal challenges<br>• Residual stress accumulation | • Microstructural heterogeneity<br>• Surface roughness at strut boundaries<br>• Residual stresses and anisotropy | • Elastoplastic models with strain hardening required<br>• Residual stresses should be incorporated<br>• Buckling-plasticity interaction and fatigue-critical modelling essential |

The comparison presented in Table 2 demonstrates that the predictive accuracy of deformation behaviour models is strongly dependent on the chosen additive manufacturing process. Approaches based on isotropic, homogenised material assumptions may be adequate for preliminary design studies but are insufficient for capturing the process-induced anisotropy, heterogeneity, and failure mechanisms inherent to AM-fabricated lattice structures. Consequently, future deformation models and optimisation frameworks must explicitly incorporate process-specific constraints and material responses to ensure reliable performance prediction and manufacturable designs. Integrating these considerations enables more robust design strategies and supports the broader adoption of cellular architectures in high-performance engineering applications.

## 7. Conclusions

- The different mechanical properties of various biological structures facilitate a wide range of designs for bioinspired lattice components that are matched to various engineering applications.
- The models built for predicting the behaviour of cellular structures can do so, but their accuracy becomes limited at particular microscales because of computational constraints, or in attempting to predict the behaviour at numerous scales concurrently. In light of this, the existing deformation behaviour models for cellular structures struggle to predict material properties such as nonlinearity, anisotropy, or viscoelasticity.
- The proposed stress–strain curve for cellular designs revealed four stages of deformation: first buckling and bending of the structure, elastic deformation during densification while buckling and bending continue, full elastic deformation, and lastly plastic deformation forming a plateau.
- Lattice structures in various engineering applications are typically built using open and closed cellular geometries.
- There are four cases of deformation likely to occur in cellular structures, namely, buckling deformation, bending deflections, transverse shear, and direct deformation.
- The combined deformation mechanisms prevailing in a loaded lattice structure are best addressed by considering the arising stresses and failure for all of them simultaneously. Thus, the increasing order of direct, bending and buckling failure stresses for the basic model (Figure 10) adopted in this paper.
- There is an absence of analytical models in the literature describing the application of the Tresca and von Mises failure criteria on lattice structures.
- The analysis of the curves showed a nonlinear relationship between lattice member thickness, length and slenderness ratio on the one hand and critical force on the other.
- The large increases in critical forces in both the horizontal and vertical members are good for optimal design of lattices, which requires balancing of desired critical forces against exponential weight-penalties incurred by increasing thickness of lattice member.
- Integrating updated deformation behaviour models and optimisation methodologies is expected to improve the effectiveness in designs of lightweight, high-performance lattice structures adopted in a wide range of engineering applications as well as realising the full capabilities of AM technologies.

**Author Contributions:** Conceptualisation, M.I.C., T.C.D. and M.M.; methodology, M.I.C.; validation, M.I.C.; formal analysis, M.I.C.; investigation, M.I.C.; writing—original draft preparation, M.I.C.; writing—review and editing, M.I.C., T.C.D., M.M. and A.M.M.; supervision, T.C.D., M.M. and A.M.M.; funding acquisition, T.C.D. and M.M. All authors have read and agreed to the published version of the manuscript.

**Funding:** This work is based on research supported by the South African Research Chairs Initiative of the Department of Science and Technology and National Research Foundation of South Africa

(Grant No. 97994 and Grant No. SARC 20150101-097994), and the Collaborative Program in Additive Manufacturing (Contract No. CSIR-NLC-CPAM-21-MOACUT-03).

**Institutional Review Board Statement:** Not applicable.

**Informed Consent Statement:** Not applicable.

**Data Availability Statement:** The raw data supporting the conclusions of this article will be made available by the authors on request.

**Conflicts of Interest:** The authors declare no conflict of interest.

## References

1. Yeo, S.J.; Oh, M.J.; Yoo, P.J. Structurally controlled cellular architectures for high-performance ultra-lightweight materials. *Adv. Mater.* **2019**, *31*, 1803670. [CrossRef]
2. Du Plessis, A.; Razavi, N.; Benedetti, M.; Murchio, S.; Leary, M.; Watson, M.; Bhate, D.; Berto, F. Properties and applications of additively manufactured metallic cellular materials: A review. *Prog. Mater. Sci.* **2022**, *125*, 100918. [CrossRef]
3. Nazir, A.; Abate, K.M.; Kumar, A.; Jeng, J.Y. A state-of-the-art review on types, design, optimization, and additive manufacturing of cellular structures. *Int. J. Adv. Manuf. Technol.* **2019**, *104*, 3489–3510. [CrossRef]
4. Du Plessis, A.; Broeckhoven, C.; Yadroitsava, I.; Yadroitsev, I.; Hands, C.H.; Kunju, R.; Bhate, D. Beautiful and functional: A review of biomimetic design in additive manufacturing. *Addit. Manuf.* **2019**, *27*, 408–427. [CrossRef]
5. Korkmaz, M.E.; Gupta, M.K.; Robak, G.; Moj, K.; Krolczyk, G.M.; Kuntoğlu, M. Development of lattice structure with selective laser melting process: A state of the art on properties, future trends and challenges. *J. Manuf. Process.* **2022**, *81*, 1040–1063. [CrossRef]
6. Song, W.; Mu, Z.; Zhang, Z.; Wang, Y.; Hu, H.; Ma, Z.; Huang, L.; Wang, Z.; Zhang, B.; Li, Y.; et al. Cross-scale biological models of species for future biomimetic composite design: A review. *Coatings* **2021**, *11*, 1297. [CrossRef]
7. Fratzl, P.; Dunlop, J.; Weinkamer, R. (Eds.) *Materials Design Inspired by Nature: Function Through Inner Architecture*; Royal Society of Chemistry: London, UK, 2015.
8. Yu, H.; Zhang, J.; Zhang, S.; Han, Z. Bionic structures and materials inspired by plant leaves: A comprehensive review for innovative problem-solving. *Prog. Mater. Sci.* **2023**, *139*, 101181. [CrossRef]
9. Siddique, S.H.; Hazell, P.J.; Wang, H.; Escobedo, J.P.; Ameri, A.A. Lessons from nature: 3D printed bio-inspired porous structures for impact energy absorption—A review. *Addit. Manuf.* **2022**, *58*, 103051. [CrossRef]
10. Chatterjee, A.; Mishra, A.; Sharma, S.; Bhagchandani, R.K. Review on lightweight materials, additive manufacturing techniques and design optimization of an airplane. In *AIP Conference Proceedings*; AIP Publishing: New York, NY, USA, 2022; Volume 2653.
11. Pan, C.; Han, Y.; Lu, J. Design and optimization of lattice structures: A review. *Appl. Sci.* **2020**, *10*, 6374. [CrossRef]
12. Zhang, W.; Xu, J. Advanced lightweight materials for Automobiles: A review. *Mater. Des.* **2022**, *221*, 110994. [CrossRef]
13. Almansoori, H.N.A. Applications of 3D-Printing in Spacecraft Structures. Master's Thesis, Khalifa University, Abu Dhabi, Saudi Arabia, 2022.
14. Xiong, C.; Dai, K.; Luo, Y.; Yang, Z.; Qiu, K.; Tang, X. Proposal and application of onshore lattice wind turbine support structure and integrated multi-scale fatigue assessment method. *Eng. Struct.* **2024**, *302*, 117314. [CrossRef]
15. Zhang, Q.; Yang, X.; Li, P.; Huang, G.; Feng, S.; Shen, C.; Han, B.; Zhang, X.; Jin, F.; Xu, F.; et al. Bioinspired engineering of honeycomb structure–Using nature to inspire human innovation. *Prog. Mater. Sci.* **2015**, *74*, 332–400. [CrossRef]
16. Velasco-Hogan, A.; Xu, J.; Meyers, M.A. Additive manufacturing as a method to design and optimize bioinspired structures. *Adv. Mater.* **2018**, *30*, 1800940. [CrossRef]
17. Libonati, F.; Buehler, M.J. Advanced structural materials by bioinspiration. *Adv. Eng. Mater.* **2017**, *19*, 1600787. [CrossRef]
18. Ramakrishna, D.; Bala Murali, G. Bio-inspired 3D-printed lattice structures for energy absorption applications: A review. *Proc. Inst. Mech. Eng. Part L J. Mater. Des. Appl.* **2023**, *237*, 503–542. [CrossRef]
19. Ren, L.; Wang, Z.; Ren, L.; Han, Z.; Liu, Q.; Song, Z. Graded biological materials and additive manufacturing technologies for producing bioinspired graded materials: An overview. *Compos. Part B Eng.* **2022**, *242*, 110086. [CrossRef]
20. Dal Poggetto, V.F. Bioinspired acoustic metamaterials: From natural designs to optimized structures. *Front. Mater.* **2023**, *10*, 1176457. [CrossRef]
21. Gao, Z.; Wang, H.; Sun, H.; Sun, T.; Wu, Y.; Leung, C.L.A.; Wang, H. Additively manufactured high-energy-absorption metamaterials with artificially engineered distribution of bio-inspired hierarchical microstructures. *Compos. Part B Eng.* **2022**, *247*, 110345. [CrossRef]
22. Yuan, X.; Chen, M.; Yao, Y.; Guo, X.; Huang, Y.; Peng, Z.; Xu, B.; Lv, B.; Tao, R.; Duan, S.; et al. Recent progress in the design and fabrication of multifunctional structures based on metamaterials. *Curr. Opin. Solid State Mater. Sci.* **2021**, *25*, 100883. [CrossRef]

23. Nazir, A.; Gokcekaya, O.; Billah, K.M.M.; Ertugrul, O.; Jiang, J.; Sun, J.; Hussain, S. Multi-material additive manufacturing: A systematic review of design, properties, applications, challenges, and 3D printing of materials and cellular metamaterials. *Mater. Des.* **2023**, *226*, 111661. [CrossRef]
24. Letov, N.; Velivela, P.T.; Sun, S.; Zhao, Y.F. Challenges and opportunities in geometric modelling of complex bio-inspired three-dimensional objects designed for additive manufacturing. *J. Mech. Des.* **2021**, *143*, 121705. [CrossRef]
25. Huang, W.; Restrepo, D.; Jung, J.Y.; Su, F.Y.; Liu, Z.; Ritchie, R.O.; McKittrick, J.; Zavattieri, P.; Kisailus, D. Multiscale toughening mechanisms in biological materials and bioinspired designs. *Adv. Mater.* **2019**, *31*, 1901561. [CrossRef] [PubMed]
26. Giorgio, I.; Spagnuolo, M.; Andreaus, U.; Scerrato, D.; Bersani, A.M. In-depth gaze at the astonishing mechanical behaviour of bone: A review for designing bio-inspired hierarchical metamaterials. *Math. Mech. Solids* **2021**, *26*, 1074–1103. [CrossRef]
27. Wu, M.S. Strategies and challenges for the mechanical modelling of biological and bio-inspired materials. *Mater. Sci. Eng. C* **2011**, *31*, 1209–1220. [CrossRef]
28. Naleway, S.E.; Porter, M.M.; McKittrick, J.; Meyers, M.A. Structural design elements in biological materials: Application to bioinspiration. *Adv. Mater.* **2015**, *27*, 5455–5476. [CrossRef]
29. Zhang, W.; Xu, J.; Yu, T.X. Dynamic behaviours of bio-inspired structures: Design, mechanisms, and models. *Eng. Struct.* **2022**, *265*, 114490. [CrossRef]
30. Lin, E.; Li, Y.; Ortiz, C.; Boyce, M.C. 3D printed, bio-inspired prototypes and analytical models for structured suture interfaces with geometrically tuned deformation and failure behaviour. *J. Mech. Phys. Solids* **2014**, *73*, 166–182. [CrossRef]
31. Tuninetti, V.; Narayan, S.; Ríos, I.; Menacer, B.; Valle, R.; Al-lehaibi, M.; Kaisan, M.U.; Samuel, J.; Oñate, A.; Pincheira, G.; et al. Biomimetic lattice structures design and manufacturing for high stress, deformation, and energy absorption performance. *Biomimetics* **2025**, *10*, 458. [CrossRef]
32. Chen, Y.; Dang, B.; Wang, C.; Wang, Y.; Yang, Y.; Liu, M.; Bi, H.; Sun, D.; Li, Y.; Li, J. Intelligent designs from nature: Biomimetic applications in wood technology. *Prog. Mater. Sci.* **2023**, *139*, 101164. [CrossRef]
33. Shashwat, S.; Zingre, K.T.; Thurairajah, N.; Kumar, D.K.; Panicker, K.; Anand, P.; Wan, M.P. A review on bioinspired strategies for an energy-efficient built environment. *Energy Build.* **2023**, *296*, 113382. [CrossRef]
34. Yao, H.B.; Fang, H.Y.; Wang, X.H.; Yu, S.H. Hierarchical assembly of micro-/nano-building blocks: Bio-inspired rigid structural functional materials. *Chem. Soc. Rev.* **2011**, *40*, 3764–3785. [CrossRef]
35. Brown, C.P.; Whaite, A.D.; MacLeod, J.M.; Macdonald, J.; Rosei, F. With great structure comes great functionality: Understanding and emulating spider silk. *J. Mater. Res.* **2015**, *30*, 108–120. [CrossRef]
36. Holland, C.; Numata, K.; Rnjak-Kovacina, J.; Seib, F.P. The biomedical use of silk: Past, present, future. *Adv. Healthc. Mater.* **2019**, *8*, 1800465. [CrossRef]
37. Bakhshandeh, B.; Nateghi, S.S.; Gazani, M.M.; Dehghani, Z.; Mohammadzadeh, F. A review on advances in the applications of spider silk in biomedical issues. *Int. J. Biol. Macromol.* **2021**, *192*, 258–271. [CrossRef] [PubMed]
38. Gu, Y.; Yu, L.; Mou, J.; Wu, D.; Zhou, P.; Xu, M. Mechanical properties and application analysis of spider silk bionic material. *e-Polymers* **2020**, *20*, 443–457. [CrossRef]
39. Wei, J.; Pan, F.; Ping, H.; Yang, K.; Wang, Y.; Wang, Q.; Fu, Z. Bioinspired additive manufacturing of hierarchical materials: From biostructures to functions. *Research* **2023**, *6*, 0164. [CrossRef] [PubMed]
40. Ding, Z.; Klein, T.; Barner-Kowollik, C.; Mirkhalaf, M. Multifunctional nacre-like materials. *Mater. Horiz.* **2023**, *10*, 5371–5390. [CrossRef]
41. Barthelat, F. Biomimetics for next generation materials. *Philos. Trans. R. Soc. A Math. Phys. Eng. Sci.* **2007**, *365*, 2907–2919. [CrossRef] [PubMed]
42. Li, M.; Li, C.; Blackman, B.R.; Eduardo, S. Mimicking nature to control bio-material surface wetting and adhesion. *Int. Mater. Rev.* **2022**, *67*, 658–681. [CrossRef]
43. Zhang, S.; Huang, J.; Chen, Z.; Lai, Y. Bioinspired special wettability surfaces: From fundamental research to water harvesting applications. *Small* **2017**, *13*, 1602992. [CrossRef]
44. Zhu, H.; Guo, Z.; Liu, W. Biomimetic water-collecting materials inspired by nature. *Chem. Commun.* **2016**, *52*, 3863–3879. [CrossRef]
45. Sharma, V.; Kumar, S.; Reddy, K.L.; Bahuguna, A.; Krishnan, V. Bioinspired functional surfaces for technological applications. *J. Mol. Eng. Mater.* **2016**, *4*, 1640006. [CrossRef]
46. Available online: https://ashevillebeecharmer.com/honey-tips/honeycomb-edible/ (accessed on 15 April 2024).
47. Ivchenko, A.V.; Sharonov, N.; Ziatdinov, R. New conceptual design of the adaptive compliant aircraft wing frame. *Eng. Sci. Technol. Int. J.* **2019**, *22*, 1149–1154. [CrossRef]
48. Fratzl, P.; Weinkamer, R. Nature's hierarchical materials. *Prog. Mater. Sci.* **2007**, *52*, 1263–1334. [CrossRef]
49. Available online: https://aerospaceamerica.aiaa.org/departments/inspired-by-fish/ (accessed on 17 April 2024).
50. Available online: https://www.greenbiz.com/article/how-our-bones-inspire-architecture-chairs-and-cars (accessed on 17 April 2024).

51. Available online: https://www.mcgill.ca/newsroom/channels/news/unbreakable-glass-inspired-seashells-333730 (accessed on 18 April 2024).
52. Yan, J.; Zhou, T.; Peng, J.; Wang, H.; Jiang, L.; Cheng, Q. Sustainable liquid metal-induced conductive nacre. *Sci. Bull.* **2024**, *69*, 913–921. [CrossRef]
53. Restrepo, V.; Martinez, R.V. Bioinspired fabrication of reconfigurable elastomeric cementitious structures using self-healing mechanical adhesives interfaces. *Mater. Des.* **2021**, *205*, 109691. [CrossRef]
54. Available online: https://www.theguardian.com/lifeandstyle/2018/oct/06/how-to-take-cuttings-cacti-alys-fowler (accessed on 18 April 2024).
55. Available online: https://www.ajupress.com/view/20211008100320681 (accessed on 18 April 2024).
56. Li, X.; Yang, Y.; Liu, L.; Chen, Y.; Chu, M.; Sun, H.; Shan, W.; Chen, Y. 3D-printed cactus-inspired spine structures for highly efficient water collection. *Adv. Mater. Interfaces* **2020**, *7*, 1901752. [CrossRef]
57. Xiao, L.; Xu, X.; Feng, G.; Li, S.; Song, W.; Jiang, Z. Compressive performance and energy absorption of additively manufactured metallic hybrid lattice structures. *Int. J. Mech. Sci.* **2022**, *219*, 107093. [CrossRef]
58. Wang, B.X.; Xu, C.; Duan, G.; Xu, W.; Pi, F. Review of broadband metamaterial absorbers: From principles, design strategies, and tunable properties to functional applications. *Adv. Funct. Mater.* **2023**, *33*, 2213818. [CrossRef]
59. Moat, R.J.; Clarke, D.J.; Carter, F.; Rust, D.; Jowers, I. A class of aperiodic honeycombs with tuneable mechanical properties. *Appl. Mater. Today* **2024**, *37*, 102127. [CrossRef]
60. Qin, R.; Wang, X.; Lu, J.; Li, Q.; Niu, H.; Zhang, X.; Chen, B. Node-locked multi-cell honeycomb for efficient energy absorption. *Int. J. Mech. Sci.* **2024**, *268*, 109028. [CrossRef]
61. Audibert, C.; Chaves-Jacob, J.; Linares, J.M.; Lopez, Q.A. Bio-inspired method based on bone architecture to optimize the structure of mechanical workspieces. *Mater. Des.* **2018**, *160*, 708–717. [CrossRef]
62. Barba, D.; Alabort, E.; Reed, R.C. Synthetic bone: Design by additive manufacturing. *Acta Biomater.* **2019**, *97*, 637–656. [CrossRef]
63. Wang, J.; Qiao, J.; Wang, J.; Zhu, Y.; Jiang, L. Bioinspired hierarchical alumina–graphene oxide–poly (vinyl alcohol) artificial nacre with optimized strength and toughness. *ACS Appl. Mater. Interfaces* **2015**, *7*, 9281–9286. [CrossRef]
64. Finnemore, A.; Cunha, P.; Shean, T.; Vignolini, S.; Guldin, S.; Oyen, M.; Steiner, U. Biomimetic layer-by-layer assembly of artificial nacre. *Nat. Commun.* **2012**, *3*, 966. [CrossRef] [PubMed]
65. Wang, J.; Yi, S.; Yang, Z.; Chen, Y.; Jiang, L.; Wong, C.P. Laser direct structuring of bioinspired spine with backward microbarbs and hierarchical microchannels for ultrafast water transport and efficient fog harvesting. *ACS Appl. Mater. Interfaces* **2020**, *12*, 21080–21087. [CrossRef] [PubMed]
66. Gupta, S.; Gnanamoorthy, R.; Kandasubramanian, B. Additive manufacturing of topology optimized multi-functional cellular framework for enhanced energy absorption. *Prog. Addit. Manuf.* **2025**, *10*, 8865–8893. [CrossRef]
67. Al Rifaie, M.; Abdulhadi, H.; Mian, A. Advances in mechanical metamaterials for vibration isolation: A review. *Adv. Mech. Eng.* **2022**, *14*, 16878132221082872. [CrossRef]
68. Qiu, N.; Ding, Y.; Guo, J.; Fang, J. Energy dissipation of sand-filled TPMS lattices under cyclic loading. *Thin-Walled Struct.* **2025**, *209*, 112848. [CrossRef]
69. Alshihabi, M.; Bilge, T.; Kayacan, M.Y.; Farooq, M.U.; Ali, S. A novel approach to recoil pad enhancement in rifles via topological design with material extrusion and SLA. *Front. Mech. Eng.* **2025**, *11*, 1653341. [CrossRef]
70. Tuninetti, V.; Castro, J.; Valle, R.; Bustos, F.; Saggionetto, E.; Garrido, C.; Oñate, A.; Salas, A.; Lanziotti, C.; Pincheira, G.; et al. Ultrahigh Damping Efficiency in Laser Powder Bed Fusion Kelvin Metamaterials for Hysteretic Applications. *Adv. Eng. Mater.* **2025**, e202502470. [CrossRef]
71. Alkhatib, S.E.; Xu, S.; Lu, G.; Karrech, A.; Sercombe, T.B. Rate-dependent behaviour of additively manufactured topology optimised lattice structures. *Thin-Walled Struct.* **2024**, *198*, 111710. [CrossRef]
72. Gibson, L.J.; Ashby, M.F.; Schajer, G.S.; Robertson, C.I. The mechanics of two-dimensional cellular materials. *Proc. R. Soc. Lond. A Math. Phys. Sci.* **1982**, *382*, 25–42. [CrossRef]
73. Zhong, H.; Song, T.; Li, C.; Das, R.; Gu, J.; Qian, M. The Gibson-Ashby model for additively manufactured metal lattice materials: Its theoretical basis, limitations and new insights from remedies. *Curr. Opin. Solid State Mater. Sci.* **2023**, *27*, 101081. [CrossRef]
74. Ashby, M.F.; Evans, A.; Fleck, N.A.; Gibson, L.J.; Hutchinson, J.W.; Wadley, H.N.G.; Delale, F. Metal foams: A design guide. *Appl. Mech. Rev.* **2001**, *54*, B105–B106. [CrossRef]
75. Chibinyani, M.I.; Dzogbewu, T.C.; Maringa, M.; Muiruri, A. Lattice Structures Built with Different Polygon Hollow Shapes: A Review on Their Analytical Modelling and Engineering Applications. *Appl. Sci.* **2024**, *14*, 1582. [CrossRef]
76. Chibinyani, M.I.; Dzogbewu, T.C.; Maringa, M.; Muiruri, A.M. Quasi-static crushing of DMLS-produced Ti6Al4V hierarchical honeycombs. *Mater. Des.* **2025**, *260*, 114993. [CrossRef]
77. Avalle, M.; Belingardi, G.; Ibba, A. Mechanical models of cellular solids: Parameters identification from experimental tests. *Int. J. Impact Eng.* **2007**, *34*, 3–27. [CrossRef]

78. Kucewicz, M.; Baranowski, P.; Małachowski, J.; Popławski, A.; Płatek, P. Modelling, and characterization of 3D printed cellular structures. *Mater. Des.* **2018**, *142*, 177–189. [CrossRef]
79. Gibson, I.J.; Ashby, M.F. The mechanics of three-dimensional cellular materials. *Proc. R. Soc. Lond. A Math. Phys. Sci.* **1982**, *382*, 43–59. [CrossRef]
80. Reda Taha, M.; Ayyub, B.M.; Soga, K.; Daghash, S.; Heras Murcia, D.; Moreu, F.; Soliman, E. Emerging technologies for resilient infrastructure: Conspectus and roadmap. *ASCE-ASME J. Risk Uncertain. Eng. Syst. Part A Civ. Eng.* **2021**, *7*, 03121002. [CrossRef]
81. Case, J.; Chilver, A.H. *Strength of Materials and Structures: An Introduction to the Mechanics of Solids and Structures*; Elsevier: Amsterdam, The Netherlands, 2013.
82. Falzon, B.G.; Aliabadi, M.F. *Buckling and Postbuckling Structures: Experimental, Analytical and Numerical Studies*; World Scientific: Singapore, 2008; Volume 1.
83. Wadee, M.A.; Bai, L. Cellular buckling in I-section struts. *Thin-Walled Struct.* **2014**, *81*, 89–100. [CrossRef]
84. Ren, R.; Ma, X.; Yue, H.; Yang, F.; Lu, Y. Stiffness enhancement methods for thin-walled aircraft structures: A review. *Thin-Walled Struct.* **2024**, *201*, 111995. [CrossRef]
85. Armstrong, C. *Mechanics of Engineering Materials*; Prentice Hall: Hoboken, NJ, USA, 1987.
86. Crawford, R.J.; Martin, P.J. *Plastics Engineering*; Butterworth-Heinemann: Oxford, UK, 2020.
87. Khan, M.; Haq, M.R.U.; Ahmed, Y.S.; Nazir, A. Advanced Mechanical Metamaterials: Hybrid Lattice Structures, Design Strategies, Multifunctionality, and Challenges for Additive Manufacturing. *Adv. Eng. Mater.* **2025**, *27*, 2500308. [CrossRef]
88. Chibinyani, M.I.; Dzogbewu, T.C.; Maringa, M.; Muiruri, A.M. Numerical modelling of DMLS Ti6Al4V (ELI) polygon structures. *Results Mater.* **2023**, *20*, 100456. [CrossRef]
89. Tuninetti, V.; Jaramillo, A.F.; Riu, G.; Rojas-Ulloa, C.; Znaidi, A.; Medina, C.; Mateo, A.M.; Roa, J.J. Experimental Correlation of Mechanical Properties of the Ti6Al4V Alloy at Different Length Scales. *Metals* **2021**, *11*, 104. [CrossRef]
90. Valle, R.; Pincheira, G.; Tuninetti, V.; Fernandez, E.; Uribe-Lam, E. Design and Characterization of Asymmetric Cell Structure of Auxetic Material for Predictable Directional Mechanical Response. *Materials* **2022**, *15*, 1841. [CrossRef]
91. Guzmán, C.F.; Tuninetti, V.; Gilles, G.; Habraken, A.M. Assessment of damage and anisotropic plasticity models to predict Ti6Al4V behavior. *Key Eng. Mater.* **2015**, *651*, 575–580. [CrossRef]
92. Moletsane, M.G.; Yadroitsava, I.; Yadroitsev, I.; Krakhmalev, P.; Kazantseva, N.; Du Plessis, A. Tensile properties and microstructure of direct metal laser-sintered Ti6Al4V (ELI) alloy. *S. Afr. J. Ind. Eng.* **2016**, *27*, 110–121. [CrossRef]
93. Van Zyl, I.; Yadroitsava, I.; Yadroitsev, I. Residual stress in Ti6Al4V objects produced by direct metal laser sintering. *S. Afr. J. Ind. Eng.* **2016**, *27*, 134–141. [CrossRef]
94. Thamae, M.; Maringa, M.; du Preez, W. A Comparative Analysis of Low and High SiC Volume Fraction Additively Manufactured SiC/Ti6Al4V (ELI) Composites Based on the Best Process Parameters of Laser Power, Scanning Speed and Hatch Distance. *Materials* **2024**, *17*, 2606. [CrossRef]
95. Dzogbewu, T.C.; du Preez, W.B. Additive manufacturing of Ti-based intermetallic alloys: A review and conceptualization of a next-generation machine. *Materials* **2021**, *14*, 4317. [CrossRef]
96. Ge, J.; Pillay, S.; Ning, H. Post-process treatments for additive-manufactured metallic structures: A comprehensive review. *J. Mater. Eng. Perform.* **2023**, *32*, 7073–7122. [CrossRef]
97. Pal, S.; Velay, X.; Saleem, W.; Rathore, M.F. Investigating the anisotropic effects on machining behavior and performance of as-built selective laser melting processed Ti6Al4V alloy. *Prog. Addit. Manuf.* **2025**, *10*, 7141–7153. [CrossRef]
98. Bedford, A.; Liechti, K.M. Criteria for Failure and Fracture. In *Mechanics of Materials*; Springer: Cham, Switzerland, 2020; pp. 823–893. [CrossRef]
99. Cunha, A.; Yanik, Y.; Olivieri, C.; da Silva, S. Tresca vs. von Mises: Which failure criterion is more conservative in a probabilistic context? *J. Appl. Mech.* **2023**, *91*, 111008. [CrossRef]
100. Barsanescu, P.D.; Comanici, A.M. von Mises hypothesis revised. *Acta Mech.* **2017**, *228*, 433–446. [CrossRef]
101. David Müzel, S.; Bonhin, E.P.; Guimarães, N.M.; Guidi, E.S. Application of the finite element method in the analysis of composite materials: A review. *Polymers* **2020**, *12*, 818. [CrossRef]
102. Erdemir, A.; Guess, T.M.; Halloran, J.; Tadepalli, S.C.; Morrison, T.M. Considerations for reporting finite element analysis studies in biomechanics. *J. Biomech.* **2012**, *45*, 625–633. [CrossRef] [PubMed]
103. Liang, L.; Liu, M.; Martin, C.; Sun, W. A deep learning approach to estimate stress distribution: A fast and accurate surrogate of finite-element analysis. *J. R. Soc. Interface* **2018**, *15*, 20170844. [CrossRef]
104. Gao, J.; Luo, Z.; Li, H.; Gao, L. Topology optimization for multiscale design of porous composites with multi-domain microstructures. *Comput. Methods Appl. Mech. Eng.* **2019**, *344*, 451–476. [CrossRef]
105. Maconachie, T.; Leary, M.; Lozanovski, B.; Zhang, X.; Qian, M.; Faruque, O.; Brandt, M. SLM lattice structures: Properties, performance, applications and challenges. *Mater. Des.* **2019**, *183*, 108137. [CrossRef]
106. Ojha, M.; Singh, K.P.; Chakraborty, P.; Verma, S. A review of multi-objective optimisation and decision making using evolutionary algorithms. *Int. J. Bio-Inspired Comput.* **2019**, *14*, 69–84. [CrossRef]

107. Deb, K. Multi-objective optimisation using evolutionary algorithms: An introduction. In *Multi-Objective Evolutionary Optimisation for Product Design and Manufacturing*; Springer: London, UK, 2011; pp. 3–34.
108. De Buck, V.; López, C.A.M.; Nimmegeers, P.; Hashem, I.; Van Impe, J. Multi-objective optimisation of chemical processes via improved genetic algorithms: A novel trade-off and termination criterion. In *Computer Aided Chemical Engineering*; Elsevier: Amsterdam, The Netherlands, 2019; Volume 46, pp. 613–618.
109. Hartloper, A.R.; de Castro e Sousa, A.; Lignos, D.G. Constitutive modeling of structural steels: Nonlinear isotropic/kinematic hardening material model and its calibration. *J. Struct. Eng.* **2021**, *147*, 04021031. [CrossRef]
110. De Angelis, F.; Cancellara, D.; Grassia, L.; D'Amore, A. The influence of loading rates on hardening effects in elasto/viscoplastic strain-hardening materials. *Mech. Time-Depend. Mater.* **2018**, *22*, 533–551. [CrossRef]
111. Swain, D.; Selvan, S.K.; Thomas, B.P.; Asraff, A.K.; Philip, J. A full-range stress-strain model for metallic materials depicting non-linear strain-hardening behavior. *J. Strain Anal. Eng. Des.* **2021**, *56*, 291–312. [CrossRef]
112. Ren, X.; Xiao, L.; Hao, Z. Multi-property cellular material design approach based on the mechanical behaviour analysis of the reinforced lattice structure. *Mater. Des.* **2019**, *174*, 107785. [CrossRef]
113. Obadimu, S.O.; Kourousis, K.I. Compressive behaviour of additively manufactured lattice structures: A review. *Aerospace* **2021**, *8*, 207. [CrossRef]
114. Hanks, B.; Berthel, J.; Frecker, M.; Simpson, T.W. Mechanical properties of additively manufactured metal lattice structures: Data review and design interface. *Addit. Manuf.* **2020**, *35*, 101301. [CrossRef]
115. Asami, K.; Roth, S.; Krukenberg, M.; Röver, T.; Herzog, D.; Emmelmann, C. Predictive modeling of lattice structure design for 316L stainless steel using machine learning in the L-PBF process. *J. Laser Appl.* **2023**, *35*, 042046. [CrossRef]
116. Goh, G.D.; Sing, S.L.; Yeong, W.Y. A review on machine learning in 3D printing: Applications, potential, and challenges. *Artif. Intell. Rev.* **2021**, *54*, 63–94.
117. Pais, A.; Alves, J.L.; Jorge, R.N.; Belinha, J. Multiscale homogenization techniques for TPMS foam material for biomedical structural applications. *Bioengineering* **2023**, *10*, 515. [CrossRef] [PubMed]
118. Luo, T.; Wang, L.; Liu, F.; Chen, M.; Li, J. Modal response improvement of periodic lattice materials with a shear modulus-based FE homogenized model. *Materials* **2024**, *17*, 1314. [CrossRef]
119. Feng, C.; Yang, R.; Niu, B.; Meng, X. DDSM: Design-Oriented Dual-Scale Shape-Material Model for Lattice Material Components. *Materials* **2022**, *15*, 7428. [CrossRef]
120. Dal Fabbro, P.; Rosso, S.; Ceruti, A.; Boscolo Bozza, D.; Meneghello, R.; Concheri, G.; Savio, G. Analysis of a preliminary design approach for conformal lattice structures. *Appl. Sci.* **2021**, *11*, 11449. [CrossRef]
121. Ráž, K.; Chval, Z.; Pereira, M. Lattice structures—Mechanical description with respect to additive manufacturing. *Materials* **2024**, *17*, 5298. [CrossRef]
122. Debreceni, A.; Buri, Z.; Bodzás, S. Linking Process Parameters, Structure, and Properties in Material Extrusion Additive Manufacturing of Polymers and Composites: A Review. *J. Manuf. Mater. Process.* **2025**, *9*, 286. [CrossRef]
123. Dai, S.; Zhu, K.; Wang, S.; Deng, Z. Additively manufactured materials: A critical review on their anisotropic mechanical properties and modeling methods. *J. Manuf. Process.* **2025**, *141*, 789–814. [CrossRef]
124. Guo, X.; Wang, E.; Yang, H.; Zhai, W. Mechanical characterization and constitutive modeling of additively-manufactured polymeric materials and lattice structures. *J. Mech. Phys. Solids* **2024**, *189*, 105711. [CrossRef]
125. Tang, T.; Wang, L.; Zhu, M.; Zhang, H.; Dong, J.; Yue, W.; Xia, H. Topology Optimization: A Review for Structural Designs Under Statics Problems. *Materials* **2024**, *17*, 5970. [CrossRef]
126. Zhao, D.; Wang, H. Topology optimization of compliant mechanisms considering manufacturing uncertainty, fatigue, and static failure constraints. *Processes* **2023**, *11*, 2914. [CrossRef]
127. da Silva, G.A.; Emmendoerfer, H., Jr. Fail-safe stress-constrained manufacturing error tolerant topology optimization. *Comput. Methods Appl. Mech. Eng.* **2024**, *421*, 116817. [CrossRef]
128. Somnic, J.; Jo, B.W. Homogenization methods of lattice materials. *Encyclopedia* **2022**, *2*, 1091–1102. [CrossRef]
129. Cunha, F.G.; Santos, T.G.; Xavier, J. In situ monitoring of additive manufacturing using digital image correlation: A review. *Materials* **2021**, *14*, 1511. [CrossRef]
130. Mousa, M.A.; Yussof, M.M.; Hussein, T.S.; Assi, L.N.; Ghahari, S. A digital image correlation technique for laboratory structural tests and applications: A systematic literature review. *Sensors* **2023**, *23*, 9362. [CrossRef] [PubMed]
131. AbouelNour, Y.; Gupta, N. In-situ monitoring of sub-surface and internal defects in additive manufacturing: A review. *Mater. Des.* **2022**, *222*, 111063. [CrossRef]
132. Ngo, T.D.; Kashani, A.; Imbalzano, G.; Nguyen, K.T.; Hui, D. Additive manufacturing (3D printing): A review of materials, methods, applications and challenges. *Compos. Part B Eng.* **2018**, *143*, 172–196. [CrossRef]
133. Sun, J.; Gu, H.; Zhang, J.; Dai, G.; Li, B.; Sun, Z.; Liang, Z. Compressive Mechanical Properties of Lattice Structures with Varied Structural Parameters Prepared by Stereolithography. *Materials* **2025**, *18*, 3898. [CrossRef]

134. Tymrak, B.M.; Kreiger, M.; Pearce, J.M. Mechanical properties of components fabricated with open-source 3-D printers under realistic environmental conditions. *Mater. Des.* **2014**, *58*, 242–246. [CrossRef]
135. Chacón, J.M.; Caminero, M.A.; García-Plaza, E.; Núnez, P.J. Additive manufacturing of PLA structures using fused deposition modelling: Effect of process parameters on mechanical properties and their optimal selection. *Mater. Des.* **2017**, *124*, 143–157. [CrossRef]
136. Chen, H.; Guo, L.; Zhu, W.; Li, C. Recent advances in multi-material 3D printing of functional ceramic devices. *Polymers* **2022**, *14*, 4635. [CrossRef]
137. DebRoy, T.; Wei, H.L.; Zuback, J.S.; Mukherjee, T.; Elmer, J.W.; Milewski, J.O.; Beese, A.M.; Wilson-Heid, A.; De, A.; Zhang, W. Additive manufacturing of metallic components–process, structure and properties. *Prog. Mater. Sci.* **2018**, *92*, 112–224. [CrossRef]
138. Guo, Z.; Ma, Y.; Ali, T.; Yang, Y.; Hou, J.; Li, S.; Wang, H. Enhanced Compressive Properties of Additively Manufactured Ti6Al4V Gradient Lattice Structures. *Metals* **2025**, *15*, 230. [CrossRef]

**Disclaimer/Publisher's Note:** The statements, opinions and data contained in all publications are solely those of the individual author(s) and contributor(s) and not of MDPI and/or the editor(s). MDPI and/or the editor(s) disclaim responsibility for any injury to people or property resulting from any ideas, methods, instructions or products referred to in the content.